Distinguishing Exotic States from Scattering States in Lattice QCD

by

Dmitry Sigaev

Submitted to the Department of Physics
in partial fulfillment of the requirements for the degree of

Doctor of Philosophy in Physics

at the

MASSACHUSETTS INSTITUTE OF TECHNOLOGY

June 2008

Author . . . .
Department of Physics
May 19, 2008

Certified by . . . . .
John W. Negele
Professor of Physics
Thesis Supervisor

Accepted by . . . .
Thomas J. Greytak
Associate Department Head for Education, Professor of Physics

Distinguishing Exotic States from Scattering States in Lattice QCD

by

Dmitry Sigaev

Abstract

This work explores the problem of distinguishing potentially interesting new exotic states in QCD from conventional scattering states using lattice QCD, and addresses the specific case of the search for localized resonances in a system of five quarks. We employ a complete basis of local interpolating operators, as well as a number of spatially distributed operators, to search for localized resonances in the system of five quarks. Motivated by initially promising experimental searches for the $\Theta^+(1540)$ pentaquark, we have set out to implement new approaches, both on the theoretical and computational side, to allow for calculations deemed infeasible by other groups searching for pentaquarks on the lattice. We restrict our system of five quarks to the quantum numbers of the $\Theta^+(1540)$ pentaquark and get an insight into the structure of its states, calculate their energies and explore their properties. Finally, we use the obtained results to discriminate between scattering and exotic states. The calculation is performed in the quenched approximation with heavy Wilson fermions.

Thesis Supervisor: John W. Negele
Title: Professor of Physics

Acknowledgments

Contents

List of Figures

List of Tables

Chapter 1

Introduction

Supported by vast experimental evidence, quantum chromodynamics has been established as the correct theory of strong interactions for decades. Looking at its remarkably simple Lagrangian, one could hope that many aspects of it can be easily developed and understood. However, despite the seeming simplicity and constant effort of the world's best talent, QCD has so far eluded exhaustive mathematical explanation. Its significance and difficulty is well illustrated by the fact that one of its fundamental challenges, proving confinement, is among the seven Millennium Prize Problems selected by the scientific advisory board of the Clay Mathematics Institute.

We take as a starting line the spectroscopy arm of quantum chromodynamics. One of the things that theorists have long sought was bound states that would not fall into the category of either a quark-antiquark meson or a three-quark baryon. Nothing explicitly prohibits such states, called exotic for their rarity, in the fundamentals of QCD. Nonetheless, not a single experimental observation has confirmed their existence for many years, adding up to the list of QCD mysteries.

That's why the apparent observation of the Θ^+ particle with minimal quark content $uudd\bar{s}$ created tremendous interest in high-energy and nuclear physics. Upon solid confirmation, this particle could pave the way to a manifold of other exotics, ultimately taking us significantly further in our understanding of QCD.

However, reality has put this plan to a serious test. As the flurry of experimental searches following the original discovery was running into problems trying to con-

firm the observation, the effort on the part of lattice QCD theorists reflected that spirit, yielding inconclusive, ambiguous calculations. Lattice theorists were facing a multitude of problems, most of them new and unexpected. Major ones were correct identification of localized narrow resonances, weeding out scattering states from the spectrum, and the enormous computational cost of the new calculation. Taking the analogous baryon spectroscopy calculations as a start, one would expect to keep the cost under control as it has been low by the lattice QCD standards. However, group theory results for pentaquark spectroscopy has set a remarkably different scale on such calculations, forcing most LQCD collaborations to compromise by employing non-physical cost-reduction recipes.

Hence, in this work we have developed a thorough theoretical approach to the issues unique to lattice pentaquark spectroscopy. We explore a few sets of interpolating operators, including a complete basis of local interpolating operators, in high-statistics, high-cost calculations.

1.1   Background and context

Studies of what we would now call exotics began as early as the late 1950's, before the introduction of quarks, when the $KN(K^+p)$ system was explored. The area had attracted an increasing amount of attention through the 1970's as it was realized that three quarks cannot produce $S = +1$ baryon resonances, or Z-resonances. Considerable experimental effort was going into the area. The experimental activity was dying out, however, as no positive results were found.

Robert Jaffe suggested the possible existence of pentaquarks in 1977. Then in the early 1980's Lipkin considered the $uuds\bar{c}$ pentaquark, while the Θ^+ emerged in 1983 with new developments of the Skyrme model, a low-energy approximation to large N_c QCD. The latter, while not applying directly to the real world, is remarkably close in many features to real-world QCD. In the Skyrme model and a more general class of chiral soliton models, the baryons are associated with solitons, while the fundamental degrees of freedom are non-linearly coupled quasi-Goldstone $SU(3)_f$ pseudoscalars. In

the chiral soliton models, the second excited state soliton is a $\frac{1}{2}^{+} SU(3)_f$ antidecuplet requiring more than 3 quarks to construct. The first two states are a $\frac{1}{2}^{+} SU(3)_f$ octet and a $\frac{3}{2}^{+} SU(3)_f$ decuplet.

The mass of the antidecuplet's lightest member was estimated at roughly 1540 MeV, although the fact that it cannot be constructed out of 3 quarks was widely perceived as a fundamental flaw in the model as no such states had been experimentally found. There was, however, one paper by Diakonov, Petrov and Polyakov [1], appearing in 1997, that had a different view. Assuming the model is valid despite the lack of experimental evidence, they calculated masses and widths of various members of the antidecuplet. The important lesson learned from the calculation was that the lightest state had a width of less than 15 MeV, making it feasible to hope for its experimental observation. This anomalously narrow state inspired more theoretical papers on the subject and the first experiment in Japan.

One of the most counter-intuitive predictions of the chiral soliton models is that Θ^+, containing one anti-strange quark, is actually lighter than any non-strange members of the antidecuplet. This follows from the $SU(3)$ breaking in the antidecuplet being linear in hypercharge, a property analogous to that of the baryon decuplet.

We can illustrate this as follows. All states in the antidecuplet can be generated from $|\Theta^+\rangle = |uudd\bar{s}\rangle$ by applying a U-spin lowering operator which replaces d by s: $U_-|d\rangle = |s\rangle, U_-|\bar{s}\rangle = -|\bar{d}\rangle$. This would give us the non-strange member N^* after the first iteration, eliminating the anti-strange quark:

$$|N^*\rangle = U_-|uudd\bar{s}\rangle = -\sqrt{\frac{1}{3}}|uud\,d\bar{d}\rangle + \sqrt{\frac{2}{3}}|uud\,s\bar{s}\rangle. \tag{1.1}$$

Thus, N^* being heavier is no longer a mystery as its wave function contains a strange-anti-strange pair in one of its components. Its net strangeness is, of course, zero, while its mass is higher compared to Θ^+ by approximately $2 \times \left(\sqrt{2/3}\right)^2 - 1 = 1/3$ of the mass of the strange quark.

That's why the first experiment based on photo-production on Carbon at LEPS-C [7] targeted specifically Θ^+. Positive results were reported, generating considerable

excitement in high-energy and nuclear physics. The state was observed at 4.6σ with the mass of 1.54(1) GeV and width of less than 25 MeV. Naturally, it inspired many more experimental searches and theoretical developments. The role of providing an exhaustive QCD analysis of the pentaquarks, however, rested with lattice QCD. It was understood that the analysis was a difficult problem requiring considerable time, since sorting out unstable resonances in lattice QCD is notoriously tedious. The main problem of filtering out scattering states is especially difficult for Θ^+ as it lies above the scattering state KN and is thus shadowed by the corresponding tower of states.

Positive results in a variety of channels started pouring in after the initial discovery of Θ^+. Somewhat miraculously, however, much of the independently collected experimental evidence is now suspect as the three-star status of Θ^+ in the 2004 *Review of Particle Properties* has been downgraded to one star in the 2006 edition and omitted from the summary table [2]. We review the history and status briefly here and refer readers to other experimental reviews [3, 4, 5, 6] for details, with Fig. 1 of Ref. [4] being particularly useful.

The initial positive experimental report at LEPS-C was followed by a positive result in photo-production on Deuterium at CLAS [9] and LEPS [10]. A subsequent high-statistics measurement at CLAS [8] in a similar setting was negative. In photo-production from the proton, the initial positive result in the $\pi^+\pi^- K^+(n)$ channel at SAPHIR was not confirmed at CLAS [13], but a positive result in the $\pi^+ K^- K^+(n)$ at CLAS [14] is one of three surviving candidates. In $K^+ + n$ scattering, the positive result at DIANA [15] was followed by a negative result at BELLE [16]. A second surviving candidate is the reaction $pp \rightarrow \Sigma^+\Theta^+$ using time-of-flight at COSY [17]. In scattering electromagnetic probes at higher energy, positive e^+d results at HERMES [18] were followed by negative results with higher statistics form BaBar [20, 21], but the positive $e + p$ results at ZEUS [19] still stands as the third candidate. Re-analysis of five neutrino bubble chamber experiments at CERN and Fermilab yielded evidence of a pentaquark peak but also unexplained excess events at higher masses. Hadronic probes at high energy have also yielded mixed results, with SVD-2 reporting a positive signal for protons on nuclei [22, 23], but with negative results for Σ^- on

nuclei by WA-89 [24] and for protons on nuclei by SPHINX [25], HyperCP [26], and HERA-B [27]. Additional negative searches were reported by BES [28], CDF [29], and ALEPH [30]. The present status [6] is that a number of early observations have been refuted by subsequent measurements, the three surviving first generation experiments mentioned above and second generation results at LEPS and SVD-2 are still positive, and new analyses and measurements underway at COSY, HERMES, KEK, LEPS, CLAS, H1, and ZEUS should bring further clarity.

Although models, such as the chiral soliton models [1] or diquark model [31] are a valuable exploratory tool in suggesting exotic states, the only quantitative method to study them from first principles, in a model-independent way, is lattice quantum chromodynamics. Starting immediately after the first apparent observation of the Θ^+, a number of lattice QCD analyses have now been carried out [32, 33, 34, 35, 36, 37, 38, 39, 40, 41, 42, 43, 44]. However, reflecting the difficulty of the problem, the conclusions varied even more than the experimental results. We summarize the salient features and results of these lattice QCD calculations to motivate the present work.

Because of the resources required for dynamical quarks, all these calculations were carried out in the quenched approximation and used Wilson [32, 33, 37, 38, 40, 41, 42, 44], overlap [34, 35], or various improved fermion actions [36, 39, 43].

With one exception, all these works have considered at most three simple interpolating operators, or "sources", for spin-1/2 pentaquarks: the diquark source

$$\Pi^{\text{diquark}} = \epsilon_{abc}\epsilon_{bef}\epsilon_{cgh}(u^{Te}Cd^f)(u^{Tg}C\gamma_5 d^h)C\bar{s}^{Tc}, \tag{1.2}$$

the K-N source

$$\Pi^{\text{KN}} = \epsilon_{abc}(u^{Ta}C\gamma_5 d^b)\gamma_5 u^c(\bar{s}^e\gamma_5 d^e) - \epsilon_{abc}(u^{Ta}C\gamma_5 d^b)\gamma_5 d^c(\bar{s}^e\gamma_5 u^e), \tag{1.3}$$

and the color-fused K-N source

$$\Pi^{\text{cfKN}} = \epsilon_{abc}(u^{Ta}C\gamma_5 d^b)\gamma_5 u^e(\bar{s}^e\gamma_5 d^c) - \epsilon_{abc}(u^{Ta}C\gamma_5 d^b)\gamma_5 d^e(\bar{s}^e\gamma_5 u^c), \tag{1.4}$$

17

where C is the charge conjugation matrix.

The choice of operators has been motivated by their relatively small computational cost, since these three are nowhere near any possible fourth as far as computer time is concerned.

Reference [40] also considers a spatially displaced $K - N$ source and a spatially displaced source composed of two "good" diquarks of the form $(u^T C \gamma_5 d)$. This form is favored by the most attractive channel of the one-gluon exchange potential or 't Hooft interaction. Although a displaced interpolating operator is always more complicated than the similar local operator, considering a small number of displacements does not lead to a significant overall computational cost increase as propagator generation remains the bottleneck consuming most resources.

Initially, there was a hope that one might distinguish localized resonance states and scattering states by using diquark or fused sources having a small overlap with $K - N$ scattering states, and the $K - N$ source having a large overlap with it respectively, and hence observe states of interest in diagonal matrix elements [32, 33, 35, 36, 37, 39]. A more general approach is to diagonalize the correlation matrix in the space generated by several sources, with the hope that it will contain and distinguish both resonant and scattering states, and several works calculated in the space of two [38, 41, 42, 43], three [34], and five [40] sources. One limitation is the fact that the basis must be somewhat larger than the number of states that one expects to accurately approximate physical eigenstates.

The most common criterion for distinguishing scattering states and resonances was comparing the volume dependence of the calculated energies with those determined using the calculated N and K masses and the lowest momenta on the periodic lattice, and in the majority of cases, the results were consistent with scattering states. Reference [36] also showed that when the boundary conditions were changed to shift the $K - N$ energy but not the Θ^+ energy, the energy of the would-be resonance also shifted, indicating a scattering state. Several works considered the volume-dependence of the spectral weight, which is proportional to the overlap between the localized source and lattice eigenstate, and would vary as V^{-1} for scattering states and be volume

independent for a localized resonance. Reference [35] observed volume dependence indicating a scattering state, whereas the results in Refs. [37, 41] were roughly volume independent, compatible with a resonance. The most suggestive evidence of a resonance arises from the diagonalization of a 2×2 matrix in Refs. [38, 42]. The lowest state has a volume independent energy close to the mass of an $N + K$ and a weight $\sim V^{-1}$, indicating a $K - N$ scattering state. The excited state has an energy below the first excited $N + K$ scattering state and a volume independent weight, suggesting a resonance, but suffering from the limitation of using both states in a two-dimensional space.

1.2   Objectives

Given the limitations of lattice calculations to date, this work seeks to explore and improve pentaquark spectroscopy in several ways.

One objective is to increase the basis of pentaquark sources by systematically constructing and using all the independent local sources. Hence, we have derived below the 8 Lorentz covariant and 19 rotationally covariant operators with the quantum numbers of an isosinglet pentaquark. Although there are many equivalent bases, it is convenient and instructive to work in a basis in which pairs of light diquarks are coupled appropriately to a strange quark. Diagonalization in the full 19×19 basis allows calculation of low eigenstates without concern for the inaccuracy of the highest few states and enables study of the physical content of the various eigenstates by calculating expansion coefficients and overlaps.

Given a set of independent source operators Π_i, the conventional "variational method" for spectroscopy [45] is to calculate the correlation matrix

$$C_{ij}(t) = \langle \Pi_i(t) \Pi_j^\dagger(0) \rangle \tag{1.5}$$

and solve the generalized eigenvalue problem:

$$C_{ij}(t) u_{nj}(t, t_0) = \lambda_n(t, t_0) C_{ij}(t_0) u_{nj}(t, t_0) . \tag{1.6}$$

The time t_0 is an arbitrary reference time that is chosen in practice for numerical convenience, but in principle affects the coefficients of the eigenvectors and thus their physical interpretation. Hence, we have developed a new way to understand and remove t_0 dependence from the final physical problem. In doing so, and also in calculating overlaps between basis states and physical eigenstates, it is necessary to use the correlation matrix at equal time, $C_{ij}(0) = \langle \Pi_i(0)\Pi_j^\dagger(0) \rangle$, which requires a correction to account for the proper definition of time ordering. We then seek to utilize expansion coefficients and overlaps to understand the physical content of the calculated eigenstates and to distinguish scattering states and resonance.

In order to understand spectroscopy in the 19×19 basis as fully as possible, our numerical calculations have focused on the optimal case of heavy quark masses and very high statistics, including as many as 4672 configurations where necessary. Hence, this work necessarily postpones the physically most interesting case of light quarks in full QCD, where both instanton-based arguments and arguments based on the static one gluon exchange interaction indicate that diquark correlations and interactions will be the strongest.

The second objective is to use another capacity for extending the set of pentaquark sources by allowing them to be non-local. The possibilities here are manifold, and we cannot realistically speak of constructing a basis of operators if we allow them to be spatially distributed. Hence, we limit ourselves to the most computationally cheap operators, the KN and K^*N sources, but put their components in various spatial locations. Then we proceed analogously to the local case by combining different operators in sets and calculating the corresponding correlation matrices. The goal here is to measure scattering states populating the relevant energy region so as to compare them against the local basis results. The choice of operators is also due to our observation that K, K^* and N, mesons and baryons with the lowest energy, alone comprise a significant portion of the energy spectrum of our system of five quarks when we allow for a non-zero relative momentum. Had we added other hadrons, additional states would have appeared far above the KN threshold.

Chapter 2

Sources

In our construction of interpolating operators (sources) we do not impose any restrictions other than the right quantum numbers. We also consider only local (single-site) sources that do not have any spatial structure. We require that the sources belong to the flavor antidecuplet of states, have strangeness $S = +1$, are color singlets and have spin G_1 corresponding to continuum spin of $1/2$. The construction develops in steps.

2.1   Step 1: fixing color structure

As we have at our disposal four quarks and one antiquark, in order to form a color-singlet with the antiquark, the four quarks must couple to a color triplet. The fourfold product

$$\square^4 = \left(\begin{array}{c}\square\\\square\end{array} \oplus \square\square\right) \otimes \left(\begin{array}{c}\square\\\square\end{array} \oplus \square\square\right) \tag{2.1}$$

contains three triplets, one in each of the following products:

$$\begin{array}{c}\square\\\square\end{array} \otimes \begin{array}{c}\square\\\square\end{array} \supset \begin{array}{c}\square\square\\\square\end{array} \quad \leftrightarrow \quad \epsilon^{efg}\epsilon_{fab}\epsilon_{gcd} \, , \tag{2.2}$$

$$\begin{array}{c}\square\\\square\end{array} \otimes \square\square \supset \begin{array}{c}\square\square\\\square\end{array} \quad \leftrightarrow \quad \epsilon_{abc}\delta_d^e + \epsilon_{abd}\delta_c^e \, , \tag{2.3}$$

$$\square\square \otimes \begin{array}{c}\square\\\square\end{array} \supset \begin{array}{c}\square\square\\\square\end{array} \quad \leftrightarrow \quad \epsilon_{acd}\delta_b^e + \epsilon_{bcd}\delta_a^e \, . \tag{2.4}$$

We will need to consider all three. The first one gives a start to operators of the following form:

$$\Pi_{i\alpha j\beta k\gamma l\delta\varepsilon} = \epsilon^{efg}\epsilon_{fab}\epsilon_{gcd}\, q_{i\alpha}^a q_{j\beta}^b q_{k\gamma}^c q_{l\delta}^d s_{e\varepsilon}^{\mathrm{C}}\ , \tag{2.5}$$

where $a, \ldots$ are color indices, $i, \ldots$ flavor indices, $\alpha, \ldots$ Dirac indices and $s^{\mathrm{C}} = \bar{C}\bar{s}^{\mathrm{T}}$ with C the charge conjugation matrix. As for the other two triplets, we can use the identity

$$\epsilon_{abc}\delta_d^e + \epsilon_{abd}\delta_c^e = \epsilon^{efg}\epsilon_{fad}\epsilon_{gbc} + \epsilon^{efg}\epsilon_{fac}\epsilon_{gbd} \tag{2.6}$$

and permute quark operators to show that the resulting operators can be rewritten as $\Pi_{i\alpha l\delta j\beta k\gamma\varepsilon} + \Pi_{i\alpha k\gamma j\beta l\delta\varepsilon}$ and $\Pi_{i\alpha k\gamma j\beta l\delta\varepsilon} - \Pi_{i\alpha l\delta j\beta k\gamma\varepsilon}$, the exact same form obtained from the first triplet.

2.2 Step 2: fixing flavor structure

We want all states forming the flavor antidecuplet. The only way to achieve it is to couple the four quarks to an antisextet:

$$\boxplus \otimes \begin{array}{c}\square\\\square\end{array} \supset \boxplus\boxplus\ . \tag{2.7}$$

The same product (2.1), now interpreted in flavor space, contains two sextets, one in each of the following products

$$\begin{array}{c}\square\\\square\end{array} \otimes \begin{array}{c}\square\\\square\end{array} = \boxplus\ , \tag{2.8}$$

$$\square\square \otimes \square\square \supset \boxplus\ . \tag{2.9}$$

Since the four quarks are all light in the $S = +1$ component, we can write the corresponding operators with SU(2) flavor indices,

$$\Pi_{\alpha\beta\gamma\delta\varepsilon}^{00} = \epsilon^{ij}\epsilon^{kl}\, \epsilon^{efg}\epsilon_{fab}\epsilon_{gcd}\, q_{i\alpha}^a q_{j\beta}^b q_{k\gamma}^c q_{l\delta}^d s_{e\varepsilon}^{\mathrm{C}}\ , \tag{2.10}$$

$$\Pi_{\alpha\beta\gamma\delta\varepsilon}^{11} = (i\tau_2\tau_n)^{ij}(i\tau_2\tau_n)^{kl}\, \epsilon^{efg}\epsilon_{fab}\epsilon_{gcd}\, q_{i\alpha}^a q_{j\beta}^b q_{k\gamma}^c q_{l\delta}^d s_{e\varepsilon}^{\mathrm{C}}\ . \tag{2.11}$$

where τ_n are Pauli matrices.

Hence, we now have two general possibilities for our interpolating operators.

2.3   Step 3: fixing spin/parity

We shall now couple the Dirac indices to total spin G_1. The operator Π^{00} is antisymmetric under interchange of α and β or γ and δ, while Π^{11} is symmetric. Both are antisymmetric under interchange of the pairs (α, β) and (γ, δ). This suggests that we first couple each of the index pairs (α, β) and (γ, δ) to spin A_1 or T_1 (0 or 1 in the continuum), then couple the two pairs according to

$$A_1 \otimes A_1 = A_1 \,, \tag{2.12}$$

$$A_1 \otimes T_1 = T_1 \,, \tag{2.13}$$

$$T_1 \otimes T_1 = A_1 \oplus T_1 \oplus E \oplus T_2 \,. \tag{2.14}$$

After this, we couple the result to the antiquark. To obtain G_1, we cannot couple E and T_2, corresponding to continuum spin 2, with the G_1 of the antiquark. Therefore, the representation theory is the same as in the continuum, and so we can use continuum techniques to formulate the operators. We shall first contract pairs of indices with appropriate gamma matrices. This is where we have to lock in on a gamma matrix convention. We choose the Montvay and Münster gamma matrix convention for its computational convenience following from the diagonal form of the γ_4 matrix:

$$\gamma_i = \begin{pmatrix} 0 & -i\tau_i \\ i\tau_i & 0 \end{pmatrix}, \gamma_4 = \begin{pmatrix} 1 & 0 \\ 0 & -1 \end{pmatrix}, \gamma_5 = \gamma_1\gamma_2\gamma_3\gamma_4 = \begin{pmatrix} 0 & -1 \\ -1 & 0 \end{pmatrix},$$

$$C = \gamma_4\gamma_2 = \begin{pmatrix} 0 & -i\tau_2 \\ -i\tau_2 & 0 \end{pmatrix}, C\gamma_5 = \begin{pmatrix} i\tau_2 & 0 \\ 0 & i\tau_2 \end{pmatrix}.$$

The index pairs in Π^{00} are antisymmetric, so they can only be contracted with

the antisymmetric matrices C, $C\gamma_5$ and $C\gamma_5\gamma_\mu$, as symmetric matrices give zero. If we assume 3D-rotational covariance of the operators, antisymmetry between the two pairs leaves seven possibilities for the remaining couplings:

$$\Pi_{0\varepsilon} = \Pi^{PS}_{P\varepsilon} = \quad \epsilon^{ij}\,\epsilon^{kl}\,\epsilon^{efg}\epsilon_{fab}\epsilon_{gcd}\,(q_i^{aT}C \qquad q_j^b)\,(q_k^{cT}C\gamma_5 \quad q_l^d)\qquad (s_e^C)_\varepsilon\,, \quad (2.15)$$

$$\Pi_{1\varepsilon} = \Pi^{SS'}_{S\varepsilon} = \quad \epsilon^{ij}\,\epsilon^{kl}\,\epsilon^{efg}\epsilon_{fab}\epsilon_{gcd}\,(q_i^{aT}C\gamma_5 \quad q_j^b)\,(q_k^{cT}C\gamma_5\gamma_4 q_l^d)\,(\gamma_5\gamma_4 s_e^C)_\varepsilon\,, \quad (2.16)$$

$$\Pi_{2\varepsilon} = \Pi^{SV}_{V\varepsilon} = \quad \epsilon^{ij}\,\epsilon^{kl}\,\epsilon^{efg}\epsilon_{fab}\epsilon_{gcd}\,(q_i^{aT}C\gamma_5 \quad q_j^b)\,(q_k^{cT}C\gamma_5\gamma_p q_l^d)\,(\gamma_5\gamma_p s_e^C)_\varepsilon\,, \quad (2.17)$$

$$\Pi_{3\varepsilon} = \Pi^{PS'}_{P\varepsilon} = \quad \epsilon^{ij}\,\epsilon^{kl}\,\epsilon^{efg}\epsilon_{fab}\epsilon_{gcd}\,(q_i^{aT}C \qquad q_j^b)\,(q_k^{cT}C\gamma_5\gamma_4 q_l^d)\quad (\gamma_4 s_e^C)_\varepsilon\,, \quad (2.18)$$

$$\Pi_{4\varepsilon} = \Pi^{PV}_{A\varepsilon} = \quad \epsilon^{ij}\,\epsilon^{kl}\,\epsilon^{efg}\epsilon_{fab}\epsilon_{gcd}\,(q_i^{aT}C \qquad q_j^b)\,(q_k^{cT}C\gamma_5\gamma_p q_l^d)\quad (\gamma_p s_e^C)_\varepsilon\,, \quad (2.19)$$

$$\Pi_{5\varepsilon} = \Pi^{S'V}_{V\varepsilon} = i\,\epsilon_{pqr}\,\epsilon^{ij}\,\epsilon^{kl}\,\epsilon^{efg}\epsilon_{fab}\epsilon_{gcd}\,(q_i^{aT}C\gamma_5\gamma_4 q_j^b)\,(q_k^{cT}C\gamma_5\gamma_p q_l^d)\,(\sigma_{qr} s_e^C)_\varepsilon\,, \quad (2.20)$$

$$\Pi_{6\varepsilon} = \Pi^{VV}_{A\varepsilon} = i\,\epsilon_{pqr}\,\epsilon^{ij}\,\epsilon^{kl}\,\epsilon^{efg}\epsilon_{fab}\epsilon_{gcd}\,(q_i^{aT}C\gamma_5\gamma_p q_j^b)\,(q_k^{cT}C\gamma_5\gamma_q q_l^d)\,(\sigma_{r4} s_e^C)_\varepsilon\,, \quad (2.21)$$

where $s_e^C = \bar{C}\bar{s}^T$. Later on, we also consider an additional restriction of Lorentz-covariance, which yields four operators generated by Π^{00} instead of seven.

For Π^{11}, the possible gamma matrices are *symmetric* matrices $C\gamma_\mu$ and $C\sigma_{\mu\nu}$, where $\sigma_{\mu\nu} = \frac{i}{2}[\gamma_\mu,\gamma_\nu]$. This yields additional 12 *3D-rotationally covariant* spin couplings:

$$\Pi_{7\varepsilon} = \Pi^{P'A'}_{V\varepsilon} = \quad i\,(\tau_2\tau_n)^{ij}\,(\tau_2\tau_n)^{kl}\,\epsilon^{efg}\epsilon_{fab}\epsilon_{gcd}\,(q_i^{aT}C\gamma_4 \quad q_j^b)\,(q_k^{cT}C\sigma_{p4} q_l^d)\,(\gamma_5\gamma_p s_e^C)_\varepsilon\,,$$
$$(2.22)$$

$$\Pi_{8\varepsilon} = \Pi^{AA'}_{S\varepsilon} = \quad i\,(\tau_2\tau_n)^{ij}\,(\tau_2\tau_n)^{kl}\,\epsilon^{efg}\epsilon_{fab}\epsilon_{gcd}\,(q_i^{aT}C\gamma_p \quad q_j^b)\,(q_k^{cT}C\sigma_{p4} q_l^d)\,(\gamma_5\gamma_4 s_e^C)_\varepsilon\,,$$
$$(2.23)$$

$$\Pi_{9\varepsilon} = \Pi^{AV'}_{V\varepsilon} = \quad i\,(\tau_2\tau_n)^{ij}\,(\tau_2\tau_n)^{kl}\,\epsilon^{efg}\epsilon_{fab}\epsilon_{gcd}\,(q_i^{aT}C\gamma_p \quad q_j^b)\,(q_k^{cT}C\sigma_{pq} q_l^d)\,(\gamma_5\gamma_q s_e^C)_\varepsilon\,,$$
$$(2.24)$$

$$\Pi_{10\varepsilon} = \Pi^{P'V'}_{A\varepsilon} = i\,\epsilon_{pqr}\,(\tau_2\tau_n)^{ij}\,(\tau_2\tau_n)^{kl}\,\epsilon^{efg}\epsilon_{fab}\epsilon_{gcd}\,(q_i^{aT}C\gamma_4 \quad q_j^b)\,(q_k^{cT}C\sigma_{pq} q_l^d)\quad (\gamma_r s_e^C)_\varepsilon\,,$$
$$(2.25)$$

$$\Pi_{11\varepsilon} = \Pi^{AV'}_{P\varepsilon} = i\,\epsilon_{pqr}\,(\tau_2\tau_n)^{ij}\,(\tau_2\tau_n)^{kl}\,\epsilon^{efg}\epsilon_{fab}\epsilon_{gcd}\,(q_i^{aT}C\gamma_p \quad q_j^b)\,(q_k^{cT}C\sigma_{qr} q_l^d)\quad (\gamma_4 s_e^C)_\varepsilon\,,$$
$$(2.26)$$

Table 2.1: Norms squared at infinite quark mass of the two sets of operators used in this paper.

i	0	1	2	3	4	5	6
$n_i^2/6144$	1	1	3	1	3	3	12
$\tilde{n}_i^2/128$	6	12	6	18	9	18	36

i	7	8	9	10	11	12	13	14	15	16	17	18
$n_i^2/6144$	9	9	18	9	9	18	9	36	18	36	36	9
$\tilde{n}_i^2/128$	54	27	54	54	108	54	432	108	648	108	432	324

$$\Pi_{12\varepsilon} = \Pi_{A\varepsilon}^{AA'} = i\,\epsilon_{pqr}\,(\tau_2\tau_n)^{ij}\,(\tau_2\tau_n)^{kl}\,\epsilon^{efg}\epsilon_{fab}\epsilon_{gcd}\,(q_i^{aT}C\gamma_p\,q_j^b)\,(q_k^{cT}C\sigma_{q4}q_l^d)\quad (\gamma_r s_e^C)_\varepsilon\,,$$

$$(2.27)$$

$$\Pi_{13\varepsilon} = \Pi_{V\varepsilon}^{P'A} = i\,\epsilon_{pqr}\,(\tau_2\tau_n)^{ij}\,(\tau_2\tau_n)^{kl}\,\epsilon^{efg}\epsilon_{fab}\epsilon_{gcd}\,(q_i^{aT}C\gamma_4\,q_j^b)\,(q_k^{cT}C\gamma_p\,q_l^d)\quad (\sigma_{qr}s_e^C)_\varepsilon\,,$$

$$(2.28)$$

$$\Pi_{14\varepsilon} = \Pi_{A\varepsilon}^{AA} = i\,\epsilon_{pqr}\,(\tau_2\tau_n)^{ij}\,(\tau_2\tau_n)^{kl}\,\epsilon^{efg}\epsilon_{fab}\epsilon_{gcd}\,(q_i^{aT}C\gamma_p\,q_j^b)\,(q_k^{cT}C\gamma_q\,q_l^d)\quad (\sigma_{r4}s_e^C)_\varepsilon\,,$$

$$(2.29)$$

$$\Pi_{15\varepsilon} = \Pi_{V\varepsilon}^{A'V'} = i\,\epsilon_{pqr}\,(\tau_2\tau_n)^{ij}\,(\tau_2\tau_n)^{kl}\,\epsilon^{efg}\epsilon_{fab}\epsilon_{gcd}\,(q_i^{aT}C\sigma_{s4}q_j^b)\,(q_k^{cT}C\sigma_{ps}q_l^d)\quad (\sigma_{qr}s_e^C)_\varepsilon\,,$$

$$(2.30)$$

$$\Pi_{16\varepsilon} = \Pi_{A\varepsilon}^{V'V'} = i\,\epsilon_{pqr}\,(\tau_2\tau_n)^{ij}\,(\tau_2\tau_n)^{kl}\,\epsilon^{efg}\epsilon_{fab}\epsilon_{gcd}\,(q_i^{aT}C\sigma_{ps}q_j^b)\,(q_k^{cT}C\sigma_{qs}q_l^d)\quad (\sigma_{r4}s_e^C)_\varepsilon\,,$$

$$(2.31)$$

$$\Pi_{17\varepsilon} = \Pi_{A\varepsilon}^{A'A'} = i\,\epsilon_{pqr}\,(\tau_2\tau_n)^{ij}\,(\tau_2\tau_n)^{kl}\,\epsilon^{efg}\epsilon_{fab}\epsilon_{gcd}\,(q_i^{aT}C\sigma_{p4}q_j^b)\,(q_k^{cT}C\sigma_{q4}q_l^d)\quad (\sigma_{r4}s_e^C)_\varepsilon\,,$$

$$(2.32)$$

$$\Pi_{18\varepsilon} = \Pi_{P\varepsilon}^{A'V'} = \epsilon_{pqr}\,(\tau_2\tau_n)^{ij}\,(\tau_2\tau_n)^{kl}\,\epsilon^{efg}\epsilon_{fab}\epsilon_{gcd}\,(q_i^{aT}C\sigma_{p4}q_j^b)\,(q_k^{cT}C\sigma_{qr}q_l^d)\quad (s_e^C)_\varepsilon\,.$$

$$(2.33)$$

Imposing the additional Lorentz-covariance restriction would yield four operators that are linear combinations of the above twelve.

In order to verify linear independence of the 19 operators, we compute the inner product of the states created by the operators at infinite quark mass. We get the infinite mass by substituting delta-functions as propagators in the contractions. We

find that the operators are orthogonal (and therefore independent):

$$\langle \text{vac} | \dot{\Pi}_{i\,\varepsilon} \Pi^{\dagger}_{j\,\varepsilon'} | \text{vac} \rangle_{\infty} = \delta_{ij} \delta_{\varepsilon\varepsilon'} n_i^2 \ . \tag{2.34}$$

The norms n_i for a delta-function propagator (with unit prefactor) are given in Tab. 2.1.

All the 19 operators are products of two diquarks and an antiquark, with the diquarks of one of the following two forms:

$$Q_f(\Gamma) = \epsilon_{fab} \, \epsilon^{ij} \, (q_i^{a\mathrm{T}} C \Gamma q_j^b) \ , \tag{2.35}$$

$$Q_f^n(\Gamma) = \epsilon_{fab} \, (\tau_2 \tau_n)^{ij} \, (q_i^{a\mathrm{T}} C \Gamma q_j^b) \ , \tag{2.36}$$

e.g., the first operator can be written as

$$\Pi_{\mathrm{P}\,\varepsilon}^{\mathrm{PS}} = \epsilon^{efg} \, Q_f(1) \, Q_g(\gamma_5) \, s_e^{\mathrm{C}} \ . \tag{2.37}$$

This special form is a result of our construction. However, since the construction did not omit any operators, we have proven that all local pentaquark interpolating operators can be written in this "diquark" form. The diquarks appearing in the operators are a useful construction. In particular, there is no reason they should all be "good" diquarks in the sense that QCD interactions would lead them to play a dynamical role.

We use the diquark form for notation. Namely, the superscripts on Π indicate which spin/parity diquarks appear in each operator, while the subscript indicates to which spin/parity the two diquarks couple. The remaining ε is the free Dirac index of a spin-1/2 interpolating operator.

26

2.4 Behavior under complex conjugation

The Wilson Dirac operator has the following behavior under complex conjugation:

$$D(U)^* = C^{-1}\gamma_5 D(U^*)\gamma_5 C . \tag{2.38}$$

The above operators $\Pi_i(q, \bar{s})$ all satisfy

$$\Pi_i(q, \bar{s})^* = C^{-1}\gamma_5 \Pi_i(\gamma_5 C q^*, \bar{s}^* C^{-1}\gamma_5) . \tag{2.39}$$

Since the gauge action is real and invariant under conjugation of the gauge field and $\gamma_5 C \gamma_4^* C^{-1}\gamma_5 = \gamma_4$, it follows that the spin- (but not parity-)averaged correlator $C_{ij}^{\pm}(t) = \langle \operatorname{tr} \frac{1\pm\gamma_4}{2}\Pi_i(t)\Pi_j^{\dagger}(0)\rangle$ is real.

2.5 Operators with a definite number of upper and lower components

Having constructed a complete basis of local interpolating operators, we are free to switch to any other basis by taking linear combinations of the constructed 19 operators. As we are interested in the structure of the states, an aptly chosen basis can give us additional insight into the structure if a state looks particularly simple in the new basis. We do observe that with the following new basis inspired by the non-relativistic limit.

We choose operators with a definite number of upper and lower components in a nonrelativistic representation of the γ matrices by inserting projectors $P_\pm = \frac{1}{2}(1\pm\gamma_0)$. This mixes operators which differ only by the presence or absence of γ_4 matrices. We write the resulting operators in terms of the upper and lower components $q_\pm$ of the Dirac spinor, i.e., $q = (q_+, q_-)$ in a representation where $\gamma_4 = \operatorname{diag}(1, 1, -1, -1)$. Gamma matrices then reduce to Pauli matrices σ_m and the charge-conjugation matrix becomes $c \equiv -i\sigma_2$. The resulting (two-component) negative-parity operators are

$$\tilde{\Pi}_0^- = \epsilon^{ij}\epsilon^{kl}\,\epsilon^{efg}\epsilon_{fab}\epsilon_{gcd}\,(q_{i+}^{a\,\mathrm{T}}c\quad q_{j+}^{b})\,(q_{k+}^{c\,\mathrm{T}}c\quad q_{l-}^{d})\quad s_{e-}^{\mathrm{C}}\,, \quad (2.40)$$

$$\tilde{\Pi}_1^- = \epsilon^{ij}\epsilon^{kl}\,\epsilon^{efg}\epsilon_{fab}\epsilon_{gcd}\,(q_{i+}^{a\,\mathrm{T}}c\quad q_{j+}^{b})\,(q_{k-}^{c\,\mathrm{T}}c\quad q_{l-}^{d})\quad s_{e+}^{\mathrm{C}}\,, \quad (2.41)$$

$$\tilde{\Pi}_2^- = \epsilon^{ij}\epsilon^{kl}\,\epsilon^{efg}\epsilon_{fab}\epsilon_{gcd}\,(q_{i+}^{a\,\mathrm{T}}c\quad q_{j-}^{b})\,(q_{k-}^{c\,\mathrm{T}}c\quad q_{l-}^{d})\quad s_{e-}^{\mathrm{C}}\,, \quad (2.42)$$

$$\tilde{\Pi}_3^- = \epsilon^{ij}\epsilon^{kl}\,\epsilon^{efg}\epsilon_{fab}\epsilon_{gcd}\,(q_{i+}^{a\,\mathrm{T}}c\quad q_{j+}^{b})\,(q_{k+}^{c\,\mathrm{T}}c\sigma_m q_{l-}^{d})\,\sigma_m s_{e-}^{\mathrm{C}}\,, \quad (2.43)$$

$$\tilde{\Pi}_4^- = \epsilon^{ij}\epsilon^{kl}\,\epsilon^{efg}\epsilon_{fab}\epsilon_{gcd}\,(q_{i+}^{a\,\mathrm{T}}c\quad q_{j-}^{b})\,(q_{k+}^{c\,\mathrm{T}}c\sigma_m q_{l-}^{d})\,\sigma_m s_{e+}^{\mathrm{C}}\,, \quad (2.44)$$

$$\tilde{\Pi}_5^- = \epsilon^{ij}\epsilon^{kl}\,\epsilon^{efg}\epsilon_{fab}\epsilon_{gcd}\,(q_{i-}^{a\,\mathrm{T}}c\quad q_{j-}^{b})\,(q_{k+}^{c\,\mathrm{T}}c\sigma_m q_{l-}^{d})\,\sigma_m s_{e-}^{\mathrm{C}}\,, \quad (2.45)$$

$$\tilde{\Pi}_6^- = \mathrm{i}\,\epsilon_{mpq}\,\epsilon^{ij}\epsilon^{kl}\,\epsilon^{efg}\epsilon_{fab}\epsilon_{gcd}\,(q_{i+}^{a\,\mathrm{T}}c\sigma_m q_{j-}^{b})\,(q_{k+}^{c\,\mathrm{T}}c\sigma_p q_{l-}^{d})\,\sigma_q s_{e+}^{\mathrm{C}}\,, \quad (2.46)$$

$$\tilde{\Pi}_7^- = (\tau_2\tau_n)^{ij}(\tau_2\tau_n)^{kl}\,\epsilon^{efg}\epsilon_{fab}\epsilon_{gcd}\,(q_{i+}^{a\,\mathrm{T}}c\quad q_{j-}^{b})\,(q_{k+}^{c\,\mathrm{T}}c\sigma_m q_{l+}^{d})\,\sigma_m s_{e-}^{\mathrm{C}}\,, \quad (2.47)$$

$$\tilde{\Pi}_8^- = (\tau_2\tau_n)^{ij}(\tau_2\tau_n)^{kl}\,\epsilon^{efg}\epsilon_{fab}\epsilon_{gcd}\,(q_{i+}^{a\,\mathrm{T}}c\quad q_{j-}^{b})\,(q_{k+}^{c\,\mathrm{T}}c\sigma_m q_{l-}^{d})\,\sigma_m s_{e+}^{\mathrm{C}}\,, \quad (2.48)$$

$$\tilde{\Pi}_9^- = (\tau_2\tau_n)^{ij}(\tau_2\tau_n)^{kl}\,\epsilon^{efg}\epsilon_{fab}\epsilon_{gcd}\,(q_{i+}^{a\,\mathrm{T}}c\quad q_{j-}^{b})\,(q_{k-}^{c\,\mathrm{T}}c\sigma_m q_{l-}^{d})\,\sigma_m s_{e-}^{\mathrm{C}}\,, \quad (2.49)$$

$$\tilde{\Pi}_{10}^- = (\tau_2\tau_n)^{ij}(\tau_2\tau_n)^{kl}\,\epsilon^{efg}\epsilon_{fab}\epsilon_{gcd}\,(q_{i+}^{a\,\mathrm{T}}c\sigma_m q_{j+}^{b})\,(q_{k+}^{c\,\mathrm{T}}c\sigma_m q_{l-}^{d})\quad s_{e-}^{\mathrm{C}}\,, \quad (2.50)$$

$$\tilde{\Pi}_{11}^- = (\tau_2\tau_n)^{ij}(\tau_2\tau_n)^{kl}\,\epsilon^{efg}\epsilon_{fab}\epsilon_{gcd}\,(q_{i+}^{a\,\mathrm{T}}c\sigma_m q_{j+}^{b})\,(q_{k-}^{c\,\mathrm{T}}c\sigma_m q_{l-}^{d})\quad s_{e+}^{\mathrm{C}}\,, \quad (2.51)$$

$$\tilde{\Pi}_{12}^- = (\tau_2\tau_n)^{ij}(\tau_2\tau_n)^{kl}\,\epsilon^{efg}\epsilon_{fab}\epsilon_{gcd}\,(q_{i+}^{a\,\mathrm{T}}c\sigma_m q_{j-}^{b})\,(q_{k-}^{c\,\mathrm{T}}c\sigma_m q_{l-}^{d})\quad s_{e-}^{\mathrm{C}}\,, \quad (2.52)$$

$$\tilde{\Pi}_{13}^- = \mathrm{i}\,\epsilon_{mpq}\,(\tau_2\tau_n)^{ij}(\tau_2\tau_n)^{kl}\,\epsilon^{efg}\epsilon_{fab}\epsilon_{gcd}\,(q_{i+}^{a\,\mathrm{T}}c\sigma_m q_{j+}^{b})\,(q_{k+}^{c\,\mathrm{T}}c\sigma_p q_{l+}^{d})\,\sigma_q s_{e+}^{\mathrm{C}}\,, \quad (2.53)$$

$$\tilde{\Pi}_{14}^- = \mathrm{i}\,\epsilon_{mpq}\,(\tau_2\tau_n)^{ij}(\tau_2\tau_n)^{kl}\,\epsilon^{efg}\epsilon_{fab}\epsilon_{gcd}\,(q_{i+}^{a\,\mathrm{T}}c\sigma_m q_{j+}^{b})\,(q_{k+}^{c\,\mathrm{T}}c\sigma_p q_{l-}^{d})\,\sigma_q s_{e-}^{\mathrm{C}}\,, \quad (2.54)$$

$$\begin{aligned}
\tilde{\Pi}_{15}^- = \mathrm{i}\,\big[\quad & \epsilon_{mpq}\,(\tau_2\tau_n)^{ij}(\tau_2\tau_n)^{kl}\,\epsilon^{efg}\epsilon_{fab}\epsilon_{gcd}\,(q_{i+}^{a\,\mathrm{T}}c\sigma_m q_{j+}^{b})\,(q_{k-}^{c\,\mathrm{T}}c\sigma_p q_{l-}^{d})\quad \sigma_q s_{e+}^{\mathrm{C}} \\
+\,2\,& \epsilon_{mpq}\,(\tau_2\tau_n)^{ij}(\tau_2\tau_n)^{kl}\,\epsilon^{efg}\epsilon_{fab}\epsilon_{gcd}\,(q_{i+}^{a\,\mathrm{T}}c\sigma_m q_{j-}^{b})\,(q_{k+}^{c\,\mathrm{T}}c\sigma_p q_{l-}^{d})\quad \sigma_q s_{e+}^{\mathrm{C}}\big]\,,
\end{aligned}$$
$$(2.55)$$

$$\tilde{\Pi}_{16}^- = \mathrm{i}\,\epsilon_{mpq}\,(\tau_2\tau_n)^{ij}(\tau_2\tau_n)^{kl}\,\epsilon^{efg}\epsilon_{fab}\epsilon_{gcd}\,(q_{i+}^{a\,\mathrm{T}}c\sigma_m q_{j-}^{b})\,(q_{k-}^{c\,\mathrm{T}}c\sigma_p q_{l-}^{d})\,\sigma_q s_{e-}^{\mathrm{C}}\,, \quad (2.56)$$

$$\tilde{\Pi}_{17}^- = \mathrm{i}\,\epsilon_{mpq}\,(\tau_2\tau_n)^{ij}(\tau_2\tau_n)^{kl}\,\epsilon^{efg}\epsilon_{fab}\epsilon_{gcd}\,(q_{i-}^{a\,\mathrm{T}}c\sigma_m q_{j-}^{b})\,(q_{k-}^{c\,\mathrm{T}}c\sigma_p q_{l-}^{d})\,\sigma_q s_{e+}^{\mathrm{C}}\,, \quad (2.57)$$

$$\begin{aligned}
\tilde{\Pi}_{18}^- = \mathrm{i}\,\big[\quad & \epsilon_{mpq}\,(\tau_2\tau_n)^{ij}(\tau_2\tau_n)^{kl}\,\epsilon^{efg}\epsilon_{fab}\epsilon_{gcd}\,(q_{i+}^{a\,\mathrm{T}}c\sigma_m q_{j+}^{b})\,(q_{k-}^{c\,\mathrm{T}}c\sigma_p q_{l-}^{d})\quad \sigma_q s_{e+}^{\mathrm{C}} \\
-\,& \epsilon_{mpq}\,(\tau_2\tau_n)^{ij}(\tau_2\tau_n)^{kl}\,\epsilon^{efg}\epsilon_{fab}\epsilon_{gcd}\,(q_{i+}^{a\,\mathrm{T}}c\sigma_m q_{j-}^{b})\,(q_{k+}^{c\,\mathrm{T}}c\sigma_p q_{l-}^{d})\quad \sigma_q s_{e+}^{\mathrm{C}}\big]\,.
\end{aligned}$$
$$(2.58)$$

The positive-parity operators are obtained by flipping the strange quark parity

(i.e., interchanging s_+^C and s_-^C).

Just like the operators of the original basis, these operators are orthogonal:

$$\langle \text{vac}|\tilde{\Pi}_{i\,\varepsilon}^- \tilde{\Pi}_{j\,\varepsilon'}^{-\dagger}|\text{vac}\rangle_\infty = \delta_{ij}\delta_{\varepsilon\varepsilon'}\tilde{n}_i^2 \ , \tag{2.59}$$

with norms given in the last row of Tab. 2.1.

2.6 Relation between the bases

The two sets of operators introduced above are related as follows:

$$\tilde{\Pi}_0^- = \tfrac{1}{4}\Pi_0^- \quad -\tfrac{1}{4}\Pi_3^- \ , \tag{2.60}$$

$$\tilde{\Pi}_1^- = \tfrac{1}{2}\Pi_1^- \ , \tag{2.61}$$

$$\tilde{\Pi}_2^- = -\tfrac{1}{4}\Pi_0^- \quad -\tfrac{1}{4}\Pi_3^- \ , \tag{2.62}$$

$$\tilde{\Pi}_3^- = \tfrac{1}{4}\Pi_2^- \quad +\tfrac{1}{4}\Pi_5^- \ , \tag{2.63}$$

$$\tilde{\Pi}_4^- = -\tfrac{1}{4}\Pi_4^- \ , \tag{2.64}$$

$$\tilde{\Pi}_5^- = \tfrac{1}{4}\Pi_2^- \quad -\tfrac{1}{4}\Pi_5^- \ , \tag{2.65}$$

$$\tilde{\Pi}_6^- = \tfrac{1}{4}\Pi_6^- \ , \tag{2.66}$$

$$\tilde{\Pi}_7^- = -\tfrac{1}{4}\Pi_7^- \quad -\tfrac{1}{4}\Pi_{13}^- \ , \tag{2.67}$$

$$\tilde{\Pi}_8^- = -\tfrac{1}{4}\Pi_{10}^- \ , \tag{2.68}$$

$$\tilde{\Pi}_9^- = -\tfrac{1}{4}\Pi_7^- \quad +\tfrac{1}{4}\Pi_{13}^- \ , \tag{2.69}$$

$$\tilde{\Pi}_{10}^- = -\tfrac{1}{4}\Pi_{11}^- \quad +\tfrac{1}{4}\Pi_{18}^- \ , \tag{2.70}$$

$$\tilde{\Pi}_{11}^- = -\tfrac{1}{2}\Pi_8^- \ , \tag{2.71}$$

$$\tilde{\Pi}_{12}^- = -\tfrac{1}{4}\Pi_{11}^- \quad -\tfrac{1}{4}\Pi_{18}^- \ , \tag{2.72}$$

$$\tilde{\Pi}_{13}^- = \tfrac{1}{2}\Pi_{12}^- \quad +\tfrac{1}{4}\Pi_{14}^- -\tfrac{1}{4}\Pi_{17}^- \ , \tag{2.73}$$

$$\tilde{\Pi}_{14}^- = -\tfrac{1}{4}\Pi_9^- \quad -\tfrac{1}{4}\Pi_{15}^- \ , \tag{2.74}$$

$$\tilde{\Pi}_{15}^- = -\tfrac{1}{4}\Pi_{14}^- \quad -\tfrac{1}{2}\Pi_{16}^- -\tfrac{1}{4}\Pi_{17}^- \ , \tag{2.75}$$

$$\tilde{\Pi}_{16}^- = \tfrac{1}{4}\Pi_9^- \quad -\tfrac{1}{4}\Pi_{15}^- \ , \tag{2.76}$$

$$\tilde{\Pi}_{17}^- = -\tfrac{1}{2}\Pi_{12}^- \ + \tfrac{1}{4}\Pi_{14}^- - \tfrac{1}{4}\Pi_{17}^- \ , \tag{2.77}$$

$$\tilde{\Pi}_{18}^- = -\tfrac{1}{4}\Pi_{14}^- \ + \tfrac{1}{4}\Pi_{16}^- - \tfrac{1}{4}\Pi_{17}^- \ , \tag{2.78}$$

where Π^- denotes the negative-parity component of the four-spinor Π.

2.7 Relation to other operators

As our technique embraces all possible local operators, while most other works use three or less local operators, it is possible to write the diquark source, Π^{Diquark}, the $K - N$ source, Π^{KN}, and color-fused source, Π^{cfKN} in eqs. 1.2 - 1.4 in terms of out 19 operators:

$$\Pi^{\mathrm{Diquark}} = \tfrac{1}{4}\Pi_0 \ , \tag{2.79}$$

$$\begin{aligned}
\Pi^{\mathrm{KN}} = &-\tfrac{1}{16}\Pi_0 + \tfrac{1}{16}\Pi_1 + \tfrac{1}{16}\Pi_2 + \tfrac{1}{32}\Pi_3 \\
&+ \tfrac{1}{32}\Pi_4 + \tfrac{1}{32}\Pi_5 + \tfrac{1}{64}\Pi_6 + \tfrac{1}{32}\Pi_{10} \\
&- \tfrac{1}{32}\Pi_{11} + \tfrac{1}{32}\Pi_{12} - \tfrac{1}{32}\Pi_{13} + \tfrac{1}{64}\Pi_{14} \\
&- \tfrac{1}{32}\Pi_{15} - \tfrac{1}{64}\Pi_{16} - \tfrac{1}{64}\Pi_{17} \ ,
\end{aligned} \tag{2.80}$$

$$\begin{aligned}
\Pi^{\mathrm{cfKN}} = &\ \tfrac{1}{16}\Pi_0 - \tfrac{1}{16}\Pi_1 - \tfrac{1}{16}\Pi_2 + \tfrac{1}{32}\Pi_3 \\
&+ \tfrac{1}{32}\Pi_4 + \tfrac{1}{32}\Pi_5 + \tfrac{1}{64}\Pi_6 + \tfrac{1}{32}\Pi_{10} \\
&- \tfrac{1}{32}\Pi_{11} + \tfrac{1}{32}\Pi_{12} - \tfrac{1}{32}\Pi_{13} + \tfrac{1}{64}\Pi_{14} \\
&- \tfrac{1}{32}\Pi_{15} - \tfrac{1}{64}\Pi_{16} - \tfrac{1}{64}\Pi_{17}.
\end{aligned} \tag{2.81}$$

We see that while the diquark source is just our first operator, the two KN-inspired sources are rather long linear combinations of our operators. Expressing them in terms of our operators allows for a quick reduction of our correlation matrices to various smaller correlation matrices considered in other works.

2.8 Nucleons and kaons

Since the pentaquark is expected to be close to the N–K threshold (and what's worse, above it), it is important to identify all scattering states in the relevant energy range. We therefore measure nucleon and kaon energies, both at zero and non-zero momentum.

Lattice states are characterized by the group of lattice translations, rotations and parity, $Z^3 \rtimes {}^2O_h^-$ where ${}^2O_h^- = {}^2O \times Z_2$, with ${}^2O$ the double cover of the octahedral group and Z_2 generated by space inversion. (O_h has two double covers, $O_h^\pm$, corresponding to the two double covers $\text{Pin}_3^\pm$ of the continuum rotation group $O(3)$.) In the case of mesons with degenerate quark masses, there is also charge conjugation.

For vanishing momentum, the representations are given by those of ${}^2O_h^-$, namely A_{1P}, A_{2P}, E_P, T_{1P}, T_{2P} for bosons and G_{1P}, G_{2P} and H_P for fermions, where $P = \text{g}, \text{u}$ for even versus odd parity. We are interested in spin-1/2 pentaquark states, i.e., G_1. Local operators (which don't have orbital angular momentum) can create the kaons $A_{1,\text{g/u}}$ and $T_{1,\text{g/u}}$ corresponding to spins $0^\pm$ and $1^\pm$ and nucleons $G_{1,\text{g/u}}$ and $H_{\text{g/u}}$ corresponding to spins $\frac{1}{2}^\pm$ and $\frac{3}{2}^\pm$. We have to consider all these representations as they can all couple to G_1. Our choice of operators is given in Tab. 2.2. Charge conjugation quantum numbers are also included.

Representations with non-zero momentum $\vec{p}$ are labeled by representations of the corresponding little groups H which are given in Tab. 2.3 (see also [49, 50]). Dic_n is the dicyclic group of order $4n$, generated by a rotation r by $2\pi/n$ around the axis $\vec{p}$ and a reflection s from a plane that contains $\vec{p}$,

$$\text{Dic}_n = \langle r, s; r^{2n} = 1, r^n = s^2, rsr = s \rangle . \tag{2.82}$$

Note that s squares to -1 on fermionic states. Dic_2 is also known as the quaternion group Q_8, Dic_4 as the first generalized quaternion group Q_{16} and Dic_3 is equivalent to the semi-direct product $C_3 \rtimes C_4$ where C_4 acts on C_3 by inversion. Note that the two Dic_1 are inequivalent subgroups of ${}^2O_h^-$. The decomposition of continuum representations with helicities up to 3/2 are given in Tab. 2.4.

Table 2.2: Hadron operators for zero momentum. The superscript $\pm$ refers to charge conjugation for the cases with $m_q = m_s$. We write $\bar{s} = (\bar{s}_-, \bar{s}_+)$.

lattice rep.	continuum rep.	operator
A_{1g}^+	0^{++}	$\bar{s}q$
A_{1g}^-	0^{+-}	$\bar{s}\gamma_4 q$
A_{1u}^+	0^{-+}	$\bar{s}_+ q_+$
		$\bar{s}_- q_-$
T_{1g}^+	1^{++}	$\bar{s}_- \vec{\sigma} q_+ - \bar{s}_+ \vec{\sigma} q_-$
T_{1g}^-	1^{+-}	$\bar{s}_- \vec{\sigma} q_+ + \bar{s}_+ \vec{\sigma} q_-$
T_{1u}^-	1^{--}	$\bar{s}_+ \vec{\sigma} q_+$
		$\bar{s}_- \vec{\sigma} q_-$
G_{1g}	$\frac{1}{2}^+$	$\epsilon^{ij}(q_{i+}^{\mathrm{T}} c q_{j+})\, q_+$
		$\epsilon^{ij}(q_{i-}^{\mathrm{T}} c q_{j-})\, q_+$
		$\epsilon^{ij}(q_{i+}^{\mathrm{T}} c q_{j-})\, q_-$
G_{1u}	$\frac{1}{2}^-$	$\epsilon^{ij}(q_{i-}^{\mathrm{T}} c q_{j+})\, q_+$
		$\epsilon^{ij}(q_{i+}^{\mathrm{T}} c q_{j+})\, q_-$
		$\epsilon^{ij}(q_{i-}^{\mathrm{T}} c q_{j-})\, q_-$
H_g	$\frac{3}{2}^+$	$\epsilon^{ij}\, q_{i+}^{(\alpha} q_{j-}^{\beta} q_-^{\gamma)}$
H_u	$\frac{3}{2}^-$	$\epsilon^{ij}\, q_{i+}^{(\alpha} q_{j-}^{\beta} q_+^{\gamma)}$

Table 2.3: Little groups for non-zero momenta and normal vectors to reflection planes. $0 < a, b, c < \pi/a_{\mathrm{lat}}$ are assumed to be all different.

$\vec{p}$	H	$\hat{n}$
$(0,0,a)$	Dic_4	$(1,0,0)$
(a,a,a)	Dic_3	$(1,-1,0)/\sqrt{2}$
$(a,a,0)$	Dic_2	$(0,0,1)$
$(a,b,0)$	$\mathrm{Dic}_1 = C_4$	$(0,0,1)$
(a,a,b)	$\mathrm{Dic}_1 = C_4$	$(1,-1,0)/\sqrt{2}$
(a,b,c)	C_2	

Table 2.4: Decomposition of continuum representations with non-zero momentum into lattice representations.

$R^3 \rtimes \mathrm{Pin}^-(3)$	$\vec{p} \simeq (0,0,a)$	(a,a,a)	$(0,a,a)$	$(0,a,b), (a,a,b)$	(a,b,c)
$(p, 0^+)$	A_1	A_1	A_1	A	A
$(p, 0^-)$	A_2	A_2	A_2	B	A
$(p, \frac{1}{2})$	E_1	E_1	E	E	$2B$
$(p, 1)$	E_2	E_2	$B_1 \oplus B_2$	$A \oplus B$	$2A$
$(p, \frac{3}{2})$	E_3	$B_1 \oplus B_2$	E	E	$2B$

We use operators

$$\sum_{\vec{x}} e^{i\vec{p}\cdot\vec{x}} O(\vec{x}) \qquad (2.83)$$

with O given in Tab. 2.5. Here $\hat{n}$ is a unit normal vector to one of the planes of reflection contained in the little group and $\chi_{\pm}$ are spinors with definite helicity,

$$\hat{p}\cdot\vec{\sigma}\,\chi_{\pm} = \pm\chi_{\pm}\,. \qquad (2.84)$$

The phases are chosen such that the reflection along $\hat{n}$ maps the spinors into each other, $\chi_{-} = -i\hat{n}\cdot\vec{\sigma}\chi_{+}$. Our choice of $\hat{n}$ is included in Tab. 2.3. As in the case of local pentaquark operators, the operators are defined such that all correlators are real.

2.9 Scattering states

Once the masses of kaon and nucleon states are determined, we can make predictions for scattering states. We are interested in scattering states with total momentum zero and spin G_1. The momentum-zero component of a product of two representations with non-zero momentum is the representation induced in $^2O_h^-$ by the product of the representations of the little group,

$$([\vec{p}],\rho) \otimes ([\vec{p}],\rho') = (\vec{0}, \mathrm{Ind}^{^2O_h^-}(\rho\otimes\rho')) + \ldots (\vec{p}\neq\vec{0})\ldots\,. \qquad (2.85)$$

The induced representations of all products of a bosonic and a fermionic state from Tab. 2.4 are given in Tab. 2.6. We need to consider all pairs that have a G_1 in the last column.

2.10 Operators for scattering states

We also attempt to measure scattering states directly (instead of the single-particle states they are made of) by using product operators. For negative parity, we couple

Table 2.5: Hadron operators for non-zero momentum. For E representations, sign alternatives $\pm$ refer to the two helicity components of the representation.

$\vec{p}$	lat.rep.	cont.rep.	operator
$(0,0,p_0)$	A_2^+	0^{-+}	$\bar{s}_+ q_+$
			$\bar{s}_- q_-$
			$\bar{s}_-\hat{p}\cdot\vec{\sigma}q_+ - \bar{s}_+\hat{p}\cdot\vec{\sigma}q_-$
	A_2^-	0^{--}	$\bar{s}_-\hat{p}\cdot\vec{\sigma}q_+ + \bar{s}_+\hat{p}\cdot\vec{\sigma}q_-$
	A_1^+	0^{++}	$\bar{s}q$
	A_1^-	0^{+-}	$\bar{s}\gamma_4 q$
			$\bar{s}_+\hat{p}\cdot\vec{\sigma}q_+$
			$\bar{s}_-\hat{p}\cdot\vec{\sigma}q_-$
	E_2^+	1^+	$\pm\bar{s}_-\chi_\mp\chi_\pm^\dagger q_+ \mp \bar{s}_+\chi_\mp\chi_\pm^\dagger q_-$
	E_2^-	1^-	$\pm\bar{s}_-\chi_\mp\chi_\pm^\dagger q_+ \pm \bar{s}_+\chi_\mp\chi_\pm^\dagger q_-$
			$i\bar{s}_+\chi_\mp\chi_\pm^\dagger q_+$
			$i\bar{s}_-\chi_\mp\chi_\pm^\dagger q_-$
$(p_0,p_0,0)$	$A_1^\pm, A_2^\pm$		same as $(0,0,p_0)$
	B_1^+		$\bar{s}_-\hat{n}\cdot\vec{\sigma}q_+ - \bar{s}_+\hat{n}\cdot\vec{\sigma}q_-$
	B_1^-		$\bar{s}_-\hat{n}\cdot\vec{\sigma}q_+ + \bar{s}_+\hat{n}\cdot\vec{\sigma}q_-$
			$i\bar{s}_+\hat{p}\wedge\hat{n}\cdot\vec{\sigma}q_+$
			$i\bar{s}_-\hat{p}\wedge\hat{n}\cdot\vec{\sigma}q_-$
	B_2^+		$\bar{s}_-\hat{p}\wedge\hat{n}\cdot\vec{\sigma}q_+ - \bar{s}_+\hat{p}\wedge\hat{n}\cdot\vec{\sigma}q_-$
	B_2^-		$\bar{s}_-\hat{p}\wedge\hat{n}\cdot\vec{\sigma}q_+ + \bar{s}_+\hat{p}\wedge\hat{n}\cdot\vec{\sigma}q_-$
			$i\bar{s}_+\hat{n}\cdot\vec{\sigma}q_+$
			$i\bar{s}_-\hat{n}\cdot\vec{\sigma}q_-$
$(0,0,p_0)$	E_1	$\frac{1}{2}$	$\epsilon_{ij}\left(q_{i+}^{\mathrm{T}}cq_{j+}\right)\chi_\pm^\dagger q_+$
			$\epsilon_{ij}\left(q_{i-}^{\mathrm{T}}cq_{j-}\right)\chi_\pm^\dagger q_+$
			$\epsilon_{ij}\left(q_{i+}^{\mathrm{T}}cq_{j-}\right)\chi_\pm^\dagger q_-$
			$\pm\epsilon_{ij}\left(q_{i-}^{\mathrm{T}}cq_{j+}\right)\chi_\pm^\dagger q_+$
			$\pm\epsilon_{ij}\left(q_{i+}^{\mathrm{T}}cq_{j+}\right)\chi_\pm^\dagger q_-$
			$\pm\epsilon_{ij}\left(q_{i-}^{\mathrm{T}}cq_{j+}\right)\chi_\pm^\dagger q_-$
$(0,p_0,p_0)$	E	$\frac{1}{2}$	same as E_1

Table 2.6: Representations in $^2O_h^-$ induced by product representations of the various little groups.

$\vec{p}$	ρ	ρ'	$\mathrm{Ind}^{^2O_h^-}(\rho \otimes \rho')$
$(0,0,a)$	$A_{1,2}$	E_1	$G_{1g} \oplus G_{1u} \oplus H_g \oplus H_u$
	$B_{1,2}$	E_1	$G_{2g} \oplus G_{2u} \oplus H_g \oplus H_u$
	E_2	E_1	$G_{1g} \oplus G_{1u} \oplus G_{2g} \oplus G_{2u} \oplus 2H_g \oplus 2H_u$
	$A_{1,2}$	E_3	$G_{2g} \oplus G_{2u} \oplus H_g \oplus H_u$
	$B_{1,2}$	E_3	$G_{1g} \oplus G_{1u} \oplus H_g \oplus H_u$
	E_2	E_3	$G_{1g} \oplus G_{1u} \oplus G_{2g} \oplus G_{2u} \oplus 2H_g \oplus 2H_u$
(a,a,a)	$A_{1,2}$	$B_{1,2}$	$H_g \oplus H_u$
	E_2	$B_{1,2}$	$G_{1g} \oplus G_{1u} \oplus G_{2g} \oplus G_{2u} \oplus H_g \oplus H_u$
	$A_{1,2}$	E_1	$G_{1g} \oplus G_{1u} \oplus G_{2g} \oplus G_{2u} \oplus H_g \oplus H_u$
	E_2	E_1	$G_{1g} \oplus G_{1u} \oplus G_{2g} \oplus G_{2u} \oplus 3H_g \oplus 3H_u$
$(0,a,a)$	$A_{1,2}$	E	$G_{1g} \oplus G_{1u} \oplus G_{2g} \oplus G_{2u} \oplus 2H_g \oplus 2H_u$
	$B_{1,2}$	E	$G_{1g} \oplus G_{1u} \oplus G_{2g} \oplus G_{2u} \oplus 2H_g \oplus 2H_u$
$(0,a,b), (a,a,b)$	A	E	$G_{1g} \oplus G_{1u} \oplus G_{2g} \oplus G_{2u} \oplus 2H_g \oplus 2H_u$
	B	E	$G_{1g} \oplus G_{1u} \oplus G_{2g} \oplus G_{2u} \oplus 2H_g \oplus 2H_u$
(a,b,c)	A	B	$2G_{1g} \oplus 2G_{1u} \oplus 2G_{2g} \oplus 2G_{2u} \oplus 4H_g \oplus 4H_u$

nucleon and kaon operators to G_{1u} and isospin 0,

$$\text{NK}_{00\text{h}} = \sum_{\vec{x},m} \epsilon_{ij}\, N_{i\alpha}(\vec{x}) K_j\big(\vec{x} + \tfrac{L}{2}\vec{e}_m\big) \, , \tag{2.86}$$

$$\text{NK}_{00\text{h}}^{\star} = \sum_{\vec{x},m} \epsilon_{ij}\, \sigma_{\alpha\beta}^n N_{i\beta}(\vec{x}) K_{j,n}^{\star}\big(\vec{x} + \tfrac{L}{2}\vec{e}_m\big) \, , \tag{2.87}$$

$$\text{NK}_{0\text{hh}} = \sum_{\vec{x},m<k} \epsilon_{ij}\, N_{i\alpha}(\vec{x}) K_j\big(\vec{x} + \tfrac{L}{2}(\vec{e}_m + \vec{e}_k)\big) \, , \tag{2.88}$$

$$\text{NK}_{0\text{hh}}^{\star} = \sum_{\vec{x},m<k} \epsilon_{ij}\, \sigma_{\alpha\beta}^n N_{i\beta}(\vec{x}) K_{j,n}^{\star}\big(\vec{x} + \tfrac{L}{2}(\vec{e}_m + \vec{e}_k)\big) \, , \tag{2.89}$$

where

$$K_i = \bar{s}_+ q_{i+} \, , \tag{2.90}$$

$$K_{i,n}^{\star} = \bar{s}_+ \sigma_n q_{i+} \, , \tag{2.91}$$

$$N_{i\alpha} = \epsilon_{kl}\,(q_{k+}^{\text{T}} c q_{l+}) q_{i+\alpha} \tag{2.92}$$

are the unique K, $K^{\star}$ and N operators with only large quark components. Again, the operators have been chosen such that the correlators are real.

In momentum space,

$$\text{NK}_{00\text{h}} = \sum_{\vec{p},m} \text{e}^{-\text{i}p_m L/2} \epsilon_{ij}\, \tilde{N}_{i\alpha}(\vec{p}) \tilde{K}_j(-\vec{p}) \, , \tag{2.93}$$

$$\text{NK}_{00\text{h}}^{\star} = \sum_{\vec{p},m} \text{e}^{-\text{i}p_m L/2} \epsilon_{ij}\, \sigma_{\alpha\beta}^n \tilde{N}_{i\beta}(\vec{p}) \tilde{K}_{j,n}^{\star}(-\vec{p}) \, , \tag{2.94}$$

$$\text{NK}_{0\text{hh}} = \sum_{\vec{p},m<k} \text{e}^{-\text{i}(p_m+p_k) L/2} \epsilon_{ij}\, \tilde{N}_{i\alpha}(\vec{p}) \tilde{K}_j(-\vec{p}) \, , \tag{2.95}$$

$$\text{NK}_{0\text{hh}}^{\star} = \sum_{\vec{p},m<k} \text{e}^{-\text{i}(p_m+p_k) L/2} \epsilon_{ij}\, \sigma_{\alpha\beta}^n \tilde{N}_{i\beta}(\vec{p}) \tilde{K}_{j,n}^{\star}(-\vec{p}) \, . \tag{2.96}$$

Since $p_m = 2\pi n_m/L$, the phase factors are all ± 1. Furthermore,

$$\sum_{m<k} \text{e}^{-\text{i}(p_m+p_k) L/2} = \text{e}^{\text{i}(p_1+p_2+p_3) L/2} \sum_m \text{e}^{-\text{i}p_m L/2} \, . \tag{2.97}$$

36

The prefactor is ± 1 for even/odd $n_1 + n_2 + n_3$. Therefore, the linear combinations

$$\mathrm{NK}_{\mathrm{even}} = \mathrm{NK}_{00\mathrm{h}} + \mathrm{NK}_{0\mathrm{hh}} \ , \tag{2.98}$$

$$\mathrm{NK}_{\mathrm{odd}} = \mathrm{NK}_{00\mathrm{h}} - \mathrm{NK}_{0\mathrm{hh}} \ , \tag{2.99}$$

$$\mathrm{NK}_{00\mathrm{h}} + \mathrm{NK}_{0\mathrm{hh}} = 2 \sum_{\vec{p}\,\mathrm{even},m} \mathrm{e}^{-ip_m L/2} \epsilon_{ij}\, \tilde{N}_{i\alpha}(\vec{p}) \tilde{K}_j(-\vec{p}) \ , \tag{2.100}$$

$$\mathrm{NK}_{00\mathrm{h}} - \mathrm{NK}_{0\mathrm{hh}} = 2 \sum_{\vec{p}\,\mathrm{odd},m} \mathrm{e}^{-ip_m L/2} \epsilon_{ij}\, \tilde{N}_{i\alpha}(\vec{p}) \tilde{K}_j(-\vec{p}) \tag{2.101}$$

(and similarly for NK*) contain only components with even resp. odd relative momentum. Of course, due to nucleon-kaon interactions, all relative momenta mix. But we still expect these linear combinations to have good overlap with the corresponding scattering states. In particular, '+' should have good overlap with the zero-momentum scattering state, and '−' with the state with $\vec{p} = (0,0,p_0)$.

We use translational and rotational invariance to replace the source operators by

$$\mathrm{NK}^\circ_{00\mathrm{h}} = \epsilon_{ij}\, N_{i\alpha}(\vec{0})\, K_j\!\left(\tfrac{L}{2}\vec{e}_3\right) \ , \tag{2.102}$$

$$\mathrm{NK}^{\star\circ}_{00\mathrm{h}} = \epsilon_{ij}\, \sigma^n_{\alpha\beta} N_{i\beta}(\vec{0})\, K^\star_{j,n}\!\left(\tfrac{L}{2}\vec{e}_3\right) \ , \tag{2.103}$$

$$\mathrm{NK}^\circ_{0\mathrm{hh}} = \epsilon_{ij}\, N_{i\alpha}\!\left(\tfrac{L}{2}\vec{e}_2\right) K_j\!\left(\tfrac{L}{2}\vec{e}_3\right) \ , \tag{2.104}$$

$$\mathrm{NK}^{\star\circ}_{0\mathrm{hh}} = \epsilon_{ij}\, \sigma^n_{\alpha\beta} N_{i\beta}\!\left(\tfrac{L}{2}\vec{e}_2\right) K^\star_{j,n}\!\left(\tfrac{L}{2}\vec{e}_3\right) \ . \tag{2.105}$$

For positive parity, nucleon and kaon operators are coupled to $G_{1\mathrm{g}}$. If we only use positive parity nucleon and negative parity kaon operators, then this requires separations other than $L/2$. We use

$$\mathrm{NK}_{0\mathrm{d}0} = \sum_{\vec{x},m,\pm} \pm\epsilon_{ij}\, \sigma^m_{\alpha\beta} N_{i\beta}(\vec{x}) K_j\!\left(\vec{x} \pm 4a\vec{e}_m\right) \ , \tag{2.106}$$

$$\mathrm{NK}^{\star A_1^-}_{0\mathrm{d}0} = \sum_{\vec{x},m,\pm} \pm\epsilon_{ij}\, N_{i\alpha}(\vec{x}) K^\star_{j,m}\!\left(\vec{x} \pm 4a\vec{e}_m\right) \ , \tag{2.107}$$

$$\mathrm{NK}^{\star E_2^-}_{0\mathrm{d}0} = \sum_{\vec{x},m,k,n,\pm} \pm\epsilon_{ij}\, \epsilon_{mkn}\sigma^k_{\alpha\beta} N_{i\beta}(\vec{x}) K^\star_{j,n}\!\left(\vec{x} \pm 4a\vec{e}_m\right) \ , \tag{2.108}$$

$$\mathrm{NK_{0dh}} = \sum_{\vec{x},m\neq k,\pm} \pm\epsilon_{ij}\,\sigma^m_{\alpha\beta}N_{i\beta}(\vec{x})K_j\big(\vec{x}\pm 4a\vec{e}_m + \tfrac{L}{2}\vec{e}_k\big)\,, \tag{2.109}$$

$$\mathrm{NK_{0dh}^{\star A_1^-}} = \sum_{\vec{x},m\neq k,\pm} \pm\epsilon_{ij}\,N_{i\alpha}(\vec{x})K^{\star}_{j,m}\big(\vec{x}\pm 4a\vec{e}_m + \tfrac{L}{2}\vec{e}_k\big)\,, \tag{2.110}$$

$$\mathrm{NK_{0dh}^{\star E_2^-}} = \sum_{\vec{x},m\neq l,k,n,\pm} \pm\epsilon_{ij}\,\epsilon_{mkn}\sigma^k_{\alpha\beta}N_{i\beta}(\vec{x})K^{\star}_{j,n}\big(\vec{x}\pm 4a\vec{e}_m + \tfrac{L}{2}\vec{e}_l\big)\,. \tag{2.111}$$

Chapter 3

Spectroscopic analysis

3.1 Equal-time correlation function and the transfer matrix

We wish to extract information about energy eigenstates from the correlation matrix

$$C_{ij}^{\mathrm{E}}(t) = \langle \Pi_i(t)\Pi_j^\dagger(0)\rangle \tag{3.1}$$

obtained from a lattice simulation. Here, Π_i are the operators from Eqs. (2.15)–(2.33), projected to zero spatial momentum. In order to talk about energy spectrum and eigenstates, we have to assume that a positive transfer matrix exists. Since this is not the case for the quenched theory, the analysis presented in this chapter is, strictly speaking, only approximate.

For $t > 0$, the above correlator is equal to a matrix element

$$C_{ij}(t) = \langle \mathrm{vac}|\Pi_i e^{-\hat{H}t}\Pi_j^\dagger|\mathrm{vac}\rangle \,, \tag{3.2}$$

which is directly related to the spectrum of $\hat{H}$.

For $t = 0$, the Euclidean correlator is no longer equal to the simple matrix element (3.2), but rather to the vacuum expectation value of the normal-ordered product of

Π_i and $\Pi_j^\dagger$ [47],

$$C_{ij}^{\mathrm{E}}(0) = \langle \mathrm{vac}|N[\hat{\Pi}_i \hat{\Pi}_j^\dagger]|\mathrm{vac}\rangle \,, \tag{3.3}$$

where normal ordering is defined by its action on quark operators: in a basis where $\gamma_0 = \mathrm{diag}(1,1,-1,-1)$,

$$N[\hat{q}_{a\alpha}(\vec{x})\hat{\bar{q}}_{b\beta}(\vec{y})] = \begin{cases} \hat{q}_{a\gamma}(\vec{x})\hat{\bar{q}}_{b\beta}(\vec{y}) & \text{if } \alpha,\beta = 1,2 \\[2mm] -\hat{\bar{q}}_{b\beta}(\vec{y})\hat{q}_{a\gamma}(\vec{x}) & \text{if } \alpha,\beta = 3,4 \,. \end{cases} \tag{3.4}$$

In order to compute the matrix element (3.2) without normal-ordering, we have to sum the Euclidean expectation value over all contractions. In practice, this is achieved by replacing the naïve quark propagator at equal time by the one corresponding to a non-normalordered expectation value,

$$\begin{aligned} S'_{ai\alpha,bj\beta}(\vec{x},t;\vec{y},t') &= S_{ai\alpha,bj\beta}(\vec{x},t;\vec{y},t') \\ &+ C_{ai\alpha,bj\beta}(\vec{x},t;\vec{y},t') \,, \end{aligned} \tag{3.5}$$

where

$$\begin{aligned} C_{ai\alpha,bj\beta}(\vec{x},t;\vec{y},t') &= \hat{q}_{ai\alpha}(\vec{x},t)\hat{\bar{q}}_{bj\beta}(\vec{y},t') \\ &- N[\hat{q}_{ai\alpha}(\vec{x},t)\hat{\bar{q}}_{bj\beta}(\vec{y},t')] \end{aligned} \tag{3.6}$$

depends on the fermion action. For the Wilson action [47],

$$C_{ai\alpha,bj\beta}(\vec{x},t;\vec{y},t') = -\delta_{ij}(1-\gamma_4)_{\alpha\beta}B_{ab}^{-1}(\vec{x},\vec{y})\delta(t,t') \tag{3.7}$$

with

$$\begin{aligned} B_{ab}(\vec{x},\vec{y}) &= \delta_{ab}\delta(\vec{x},\vec{y}) \\ &- K\sum_{i=1}^{3}\left[U_i^{ab}(\vec{x})\delta(\vec{x}+\hat{\imath},\vec{y}) + U_i^{ba*}(\vec{y})\delta(\vec{x}-\hat{\imath},\vec{y})\right]. \end{aligned} \tag{3.8}$$

3.2 A variation on the traditional variational method

In order to obtain approximate energy eigenstates, one usually solves the generalized eigenvalue problem

$$C_{ij}(t)\, u_{nj}(t, t_0) = \lambda_n(t, t_0)\, C_{ij}(t_0)\, u_{nj}(t, t_0) \ , \qquad (3.9)$$

which is equivalent to the variational problem

$$\frac{\delta}{\delta u} \frac{\langle u | \mathrm{e}^{-Ht} | u \rangle}{\langle u | \mathrm{e}^{-Ht_0} | u \rangle} = 0 \ , \qquad (3.10)$$

where $|u\rangle = \sum_i \hat{\Pi}_i^\dagger |\mathrm{vac}\rangle u_i$. The solutions for different eigenvalues are orthogonal with respect to $C(t_0)$,

$$u_{ni}^* C_{ij}(t_0) u_{mj} = 0 \quad \text{if} \quad \lambda_n \neq \lambda_m \ . \qquad (3.11)$$

We shall assume in the following that there are no degeneracies.

For large t, the lowest available energy eigenstate dominates the numerator in Eq. (3.10), so the solution

$$u_n^\infty(t_0) \equiv \lim_{t \to \infty} u_n(t, t_0) \qquad (3.12)$$

maximizes the normalized overlap

$$\frac{|\langle E_n | u \rangle|}{\sqrt{\langle u | \mathrm{e}^{-Ht_0} | u \rangle}} \qquad (3.13)$$

under the constraint (3.11). It can be written as

$$|u_n^\infty\rangle = |E_n^{\mathrm{var}}\rangle - |E_m^{\mathrm{var}}\rangle M_{mm'}^{-1} \langle E_{m'}^{\mathrm{var}} | \mathrm{e}^{-Ht_0} | E_n^{\mathrm{var}}\rangle \ , \qquad (3.14)$$

where M is the $(n-1) \times (n-1)$ matrix with components

$$M_{mm'} = \langle E_m^{\mathrm{var}} | \mathrm{e}^{-Ht_0} | E_{m'}^{\mathrm{var}}\rangle \quad (m, m' = 1, \ldots, n-1) \ , \qquad (3.15)$$

and $|E_n^{\text{var}}\rangle$ is the energy eigenstate projected to the variational space,

$$|E_n^{\text{var}}\rangle = |\Pi_i\rangle C(t_0)_{ij}^{-1}\langle\Pi_j|e^{-Ht_0}|E_n\rangle \ . \tag{3.16}$$

Note that all quantities depend on t_0. The coefficients of the ground state solution, for instance, are

$$u_{0i}^{\infty}(t_0) = N_0 C(t_0)_{ij}^{-1}\langle\Pi_j|E_0\rangle \ , \tag{3.17}$$

where we have used that $|E_0\rangle$ is an eigenstate of H.

In order to eliminate this dependence, we define coefficients

$$\tilde{c}_{ni}(t, t_0) \equiv C(0)_{ij}^{-1}C(t_0)_{jk}u_{nk}(t, t_0) \ . \tag{3.18}$$

The large-t limit of $\tilde{c}_0$ is t_0-independent,

$$\tilde{c}_{0i}^{\infty} \equiv \lim_{t\to\infty}\tilde{c}_{0i}(t, t_0) = N_0 C(0)_{ij}^{-1}\langle\Pi_j|E_0\rangle \ . \tag{3.19}$$

They are the coefficients of the energy eigenstate projected to the variational space with respect to the natural metric $C_{ij}(0) = \langle\Pi_i|\Pi_j\rangle$,

$$\sum_i |\Pi_i\rangle\tilde{c}_{0i}^{\infty} = P_\Pi|E_0\rangle \ , \tag{3.20}$$

where

$$P_\Pi = |\Pi_i\rangle C(0)_{ij}^{-1}\langle\Pi_j| \ . \tag{3.21}$$

Note that, for $t_0 = 0$, the new coefficients $\tilde{c}_{0i}$ are identical to the original u_{0i}.

For excited states, an additional complication arises: the projected states $|u_n^{\infty}\rangle$, defined in (3.12), contain additional, t_0-dependent contributions from lower energy eigenstates. These introduce a t_0 dependence in $\tilde{c}_n^{\infty}$,

$$\sum_i |\Pi_i\rangle\tilde{c}_{ni}^{\infty} = P_\Pi|E_n\rangle + \sum_{m<n} P_\Pi|E_m\rangle a_{mn}(t_0) \ . \tag{3.22}$$

This t_0 dependence can be eliminated by orthogonalizing with respect to $C(0)$,

$$c_{ni}(t, t_0) \equiv \tilde{c}_{ni}(t, t_0) - \tilde{c}_{mi} A^{-1}_{mm'} \tilde{c}^*_{m'j} C_{jk}(0) \tilde{c}_{nk} , \tag{3.23}$$

where A is the $(n-1) \times (n-1)$ matrix with elements

$$A_{mm'} = \tilde{c}^*_{mi} C_{ij}(0) \tilde{c}_{m'j} \quad (m, m' = 1, \ldots, n-1) . \tag{3.24}$$

The large-t limit c^∞ of c satisfies

$$\sum_i |\Pi_i\rangle c^\infty_{ni} = P_\Pi |E_n\rangle - P_\Pi |E_m\rangle B^{-1}_{mm'} \langle E_{m'}|P_\Pi|E_n\rangle , \tag{3.25}$$

where

$$B_{mm'} = \langle E_m|P_\Pi|E_{m'}\rangle \quad (m, m' = 1, \ldots, n-1) . \tag{3.26}$$

c^∞ is t_0-independent and identical to $u^\infty(t_0{=}0)$. Explicitly,

$$\lim_{t \to \infty} c_{ni}(t, t_0) = \lim_{t \to \infty} u_{ni}(t, 0) . \tag{3.27}$$

c_n provides a means for computing the coefficient of the projected energy eigenstate $P|E_n\rangle$ from the eigenvalue problem for any t_0. This turns out to be numerically advantageous in many cases.

Note that the components of $P_\Pi|E_n\rangle$ proportional to $P_\Pi|E_m\rangle$ for $m < n$, which are lost in the orthogonalization appearing in (3.25), cannot be determined from the generalized eigenvalue problem even in principle. The corresponding components of the solution are determined solely from the requirement of orthogonality with respect to $C(t_0)$. They are, of course, present only because of the truncation to the variational space. The full energy eigenstates are orthogonal.

Chapter 4

Calculational details

A preliminary version of the numerical calculation is reported in [44]. This work improves it in several ways. We still use quenched Wilson fermions with $\beta = 6.0$ and $m_\pi = 0.90$ GeV$(\kappa_{u,d} = \kappa_s = 0.1530)$ on same two spatial sizes 16^3 and 24^3, keeping Wuppertal and APE smearing parameters intact to allow for a direct comparison with the earlier results. In regards to the improvements, first off, we increase the time extent from 32 to 64 on both spatial volumes to catch longer plateaus, thus reducing both statistical and systematical errors on our system's energy levels. Secondly, a lower light quark mass $(\kappa_{u,d} = 0.1558, m_\pi = 0.55$ GeV$)$ was included in the analysis, with the strange quark mass kept fixed. Given the different variation of the pentaquark's, meson's, and baryon's masses with the light quark mass, this offers the potential to further distinguish localized states of the pentaquark system from scattering states of a baryon and a meson. Finally, the number of configurations was increased to 4672 on a $16^3 \times 64$ lattice (only the heavier quark mass) and 1024 on a $24^3 \times 64$ lattice (both quark masses), amounting to a total of 3.2 terabytes in propagators alone.

To improve the overlap of interpolating operators with low-lying energy eigenstates, we employ Wuppertal smearing, a well-established method based on the idea of increasing the spatial extent of the source to approximate that of a typical hadron. The quark field $q(\vec{x}, t)$ is replaced in the interpolating operators with the smeared

quark field $\tilde{q}(\vec{x}, t)$, given by

$$\tilde{q}(\vec{x}, t) = \sum_{\vec{y}} W^N \left(\vec{x}, \vec{y}; \tilde{U}(t) \right) q(\vec{y}, t), \tag{4.1}$$

where

$$W \left(\vec{x}, \vec{y}; \tilde{U}(t) \right) = 1 +$$
$$\alpha \sum_{i=1}^{3} \left[\tilde{U}_i(\vec{x}) \delta(\vec{x} + \hat{\imath}, \vec{y}) + \tilde{U}_i^\dagger(\vec{y}) \delta(\vec{x} - \hat{\imath}, \vec{y}) \right]. \tag{4.2}$$

The resulting interpolating operators are then used as both sources and sinks with smearing parameters tuned to create a structure of a typical hadron's size, $N = 50$ and $\alpha = 3.0$. Note that the smearing function (4.2) includes the gauge link connections to nearest neighbors as operator B (3.8), which we employ to obtain correct equal-time correlation functions.

To maintain the physical advantage of increasing the spatial extent of the source without introducing unnecessary noise due to fluctuations of the gauge fields, it is useful to smooth the link variables in eq. (4.2) by APE smearing. We perform APE smearing of the gauge field $\tilde{U}$ entering the smearing function (4.2) with the following formula for one iteration:

$$\tilde{U}_\mu^{(1)}(x) = \mathcal{P} \left[U_\mu(x) + \rho \sum_{\nu \neq \mu} U_\nu(x) U_\mu(x + \hat{\nu}) U_\nu^\dagger(x + \hat{\mu}) \right], \tag{4.3}$$

where $\mathcal{P}$ is a projection onto $SU(3)$, which is not unique. Given an arbitrary 3×3 matrix V, we define its projection $U \in SU(3)$ by $U = V(V^\dagger V)^{-1/2} \det(V^{-1} V^\dagger)^{1/6}$ [48]. Although we continue with this choice for consistency with our preliminary report, we also consider another common choice of projection—U can also be taken to be the matrix that maximizes $\mathrm{ReTr} U V^\dagger$. Switching to the other projection turned out to have a minuscule effect on correlation functions, which was many times smaller than the statistical error. Twenty-five APE smearing steps with $\rho = 0.35$ were performed, yielding a decrease of statistical errors by a factor of two with no significant effect on

overlaps of interpolating operators with energy eigenstates.

To avoid propagation of unwanted states across the time boundaries, we apply the Dirichlet boundary condition by setting time-like gauge links to zero on the boundary before calculating propagators:

$$U_4(\vec{x}, t = -1) = 0. \tag{4.4}$$

We always put the source ten lattice spacings away from the boundary, thus compromising between a small boundary effect on equal-time correlation functions and a large fiducial volume. To simplify the notation in this presentation, we re-define t so that the source is located at $t = 0$.

Chapter 5

Optimizing contractions

In spectroscopy, the computational complexity of the problem increases dramatically with the number of quark fields and the basis dimensions. The complexity of the 19 interpolating operators creates a number of challenges in implementing the calculation of the correlation matrix. Having written the Wick contractions, we immediately notice the overwhelming number of floating point operations, and thus face the problem of reducing the number of operations by exploiting various symmetries of the matrix. Secondly, we have to devise an effective memory layout, as well as a proper order of performing those operations, so that cache misses do not delay the calculation. Finally, we have a relatively small number of operations that we are able to perform extremely efficiently, so that the program is CPU-bound. As a result, unlike most lattice calculations, where propagator generation is normally the bottleneck, straightforward calculation of the correlation matrix would take an order of magnitude more than the calculation of propagators. This situation, exacerbated by a lack of good compilers for our primary computational resources, renders low-level optimizations necessary. In the end, we have employed our own perl-based code generation to code the core of the program in the PowerPC 440d assembly, achieving sustained performance of 86% of the peak, an order of magnitude faster than what we could hope for with a C compiler.

The first 7 of the 19 operators have two isoscalar diquarks, while the other 12 have two isovector diquarks. From the implementor's point of view, this is a fundamental

difference. We, therefore, will refer to S- and V-operators, and the correlation matrix will have four blocks—SS, SV, VS, and VV—corresponding to contracting an S-operator with another S, an S with a V, and so on. It is numerically advantageous to perform sums over color indices first, leaving Dirac indices for later stages. This will conceptually reduce the bulk of the calculation to 4 massive summations over color indices, corresponding to the 4 blocks of the correlation matrix. As will be seen later, the VV block actually has all the steps needed to calculate the other 3 blocks, so we can save some operations by calculating just the VV block and storing some intermediate results for the subsequent construction of the SS, SV, and VS blocks.

The scale of the calculation is indicated by the number of operations needed for a few typical lattice tasks. Wilson propagator generation requires roughly 10 million floating point operations (FLOP) per site, taking into account the necessary number of iterations in the CG algorithm. Typical nucleon contractions need about 0.2 million FLOP per site. Classical pentaquark sources (Sasaki, KN, color-fused KN) need about 1 million FLOP per site each. In contrast, the correlation matrix comprised of the 19 operators requires 200 million FLOP per site. This really dwarfs not only typical contractions, but also propagator generation, thus becoming the new bottleneck.

We now proceed to a detailed description of our contractions.

5.1   SS block

S-operators (first 7) have the following common multiplier:

$$M^{SS\,x}_{mnop} = \varepsilon^{xfa}\varepsilon^{fde}\varepsilon^{abc}u^d_m d^e_n u^b_o d^c_p, \tag{5.1}$$

where $x, a \ldots f$ are color indices and $m \ldots p$ are Dirac indices. This multiplier has one color and four Dirac indices. We use Latin letters for Dirac indices, and since there are two sorts of these indices, it is convenient to distinguish them using upper and lower case letters. Also, the color index x is external and stays apart from the other color indices that are summed over in expressions to follow.

Now we simplify this expression:

$$
\begin{aligned}
M^{SS\,x}_{mnop} &= \varepsilon^{abc}\left(\delta^{ad}\delta^{xe} - \delta^{ae}\delta^{xd}\right)u^d_m d^e_n u^b_o d^c_p \\
&= \varepsilon^{abc}\left(u^a_m d^x_n u^b_o d^c_p - u^x_m d^a_n u^b_o d^c_p\right) \\
&= -\varepsilon^{abc}\left(u^a_m u^b_o d^x_n d^c_p - u^x_m u^b_o d^a_n d^c_p\right).
\end{aligned}
$$

The SS block of the correlation matrix includes this multiplier times the conjugated multiplier:

$$
\begin{aligned}
M^{SS}\times\overline{M^{SS}} &= \varepsilon^{abc}\varepsilon^{ABC}\left(u^a_m u^b_o d^x_n d^c_p - u^x_m u^b_o d^a_n d^c_p\right) \\
&\quad\times\left(\bar{d}^X_N \bar{d}^C_P \bar{u}^A_M \bar{u}^B_O - \bar{d}^A_N \bar{d}^C_P \bar{u}^X_M \bar{u}^B_O\right).
\end{aligned}
$$

Finally, we have the following expression:

$$
\begin{aligned}
\left\langle M^{SS}\times\overline{M^{SS}}\right\rangle &= \varepsilon^{abc}\varepsilon^{ABC}\Big[{}^{abAB}_{moMO}\cdot{}^{xcXC}_{npNP} \\
&\quad \pm\ (x\longleftrightarrow a, X\longleftrightarrow A)\Big],
\end{aligned}
\tag{5.2}
$$

where

$$
\begin{aligned}
{}^{abAB}_{mnMN} &\equiv \left\langle u^a_m u^b_n \bar{u}^A_M \bar{u}^B_N\right\rangle \equiv \left\langle d^a_m d^b_n \bar{d}^A_M \bar{d}^B_N\right\rangle \\
&\equiv L^{aB}_{mN}L^{bA}_{nM} - L^{aA}_{mM}L^{bB}_{nN},
\end{aligned}
\tag{5.3}
$$

$L^{aA}_{mM}\equiv\left\langle u^a_m \bar{u}^A_M\right\rangle$ being u- and d-quark propagator (L stands for the lower quark mass).

Form (5.2) is used in the actual calculation. The optimized calculation makes use of some symmetries of this expression. To reveal these symmetries we rewrite expression (5.2) as follows:

$$
\begin{aligned}
\left\langle M^{SS}\times\overline{M^{SS}}\right\rangle &= \varepsilon^{xfa}\varepsilon^{fde}\varepsilon^{abc}\varepsilon^{XFA}\varepsilon^{FDE}\varepsilon^{ABC} \\
&\quad\times\left({}^{dbDB}_{moMO}\cdot{}^{ecEC}_{npNP}\right).
\end{aligned}
\tag{5.4}
$$

This expression is obviously asymmetric under the replacements

$$\begin{pmatrix} m \\ n \end{pmatrix} \overset{A}{\longleftrightarrow} \begin{pmatrix} o \\ p \end{pmatrix} \tag{5.5}$$

and

$$\begin{pmatrix} M \\ N \end{pmatrix} \overset{A}{\longleftrightarrow} \begin{pmatrix} O \\ P \end{pmatrix} \tag{5.6}$$

and symmetric under the replacement

$$\begin{pmatrix} m \\ o \\ M \\ O \end{pmatrix} \overset{S}{\longleftrightarrow} \begin{pmatrix} n \\ p \\ N \\ P \end{pmatrix}. \tag{5.7}$$

Two asymmetries correspond to interchanging diquarks (we can interchange diquarks both in the source and the sink), while one symmetry corresponds to interchanging up and down quarks.

5.2   VV block

V-operators (last 12) have the following common multiplier:

$$M_{mnop}^{VV\,x} = \frac{1}{2}\varepsilon^{xfa}\varepsilon^{fde}\varepsilon^{abc}q_m^d \tau_2 \tau_n q_n^e q_o^b \tau_2 \tau_n q_p^c, \tag{5.8}$$

which is the analogue of expression (5.1) for the VV case.

Now we simplify this expression:

$$M_{mnop}^{VV\,x} = \frac{1}{2}\varepsilon^{xfa}\varepsilon^{fde}\varepsilon^{abc}$$

$$\times \left[\begin{pmatrix} u^d & d^d \end{pmatrix} \begin{pmatrix} -i & 0 \\ 0 & i \end{pmatrix} \begin{pmatrix} u^e \\ d^e \end{pmatrix} \right.$$

$$\times \begin{pmatrix} u^b & d^b \end{pmatrix} \begin{pmatrix} -i & 0 \\ 0 & i \end{pmatrix} \begin{pmatrix} u^c \\ d^c \end{pmatrix}$$

$$+ \; \begin{pmatrix} u^d & d^d \end{pmatrix} \begin{pmatrix} 1 & 0 \\ 0 & 1 \end{pmatrix} \begin{pmatrix} u^e \\ d^e \end{pmatrix}$$

$$\times \; \begin{pmatrix} u^b & d^b \end{pmatrix} \begin{pmatrix} 1 & 0 \\ 0 & 1 \end{pmatrix} \begin{pmatrix} u^c \\ d^c \end{pmatrix}$$

$$+ \; \begin{pmatrix} u^d & d^d \end{pmatrix} \begin{pmatrix} 0 & i \\ i & 0 \end{pmatrix} \begin{pmatrix} u^e \\ d^e \end{pmatrix}$$

$$\times \; \begin{pmatrix} u^b & d^b \end{pmatrix} \begin{pmatrix} 0 & i \\ i & 0 \end{pmatrix} \begin{pmatrix} u^c \\ d^c \end{pmatrix} \Bigg]$$

$$= \; \frac{1}{2} \varepsilon^{xfa} \varepsilon^{fde} \varepsilon^{abc}$$

$$\times \; \Big[- \left(-u^d u^e + d^d d^e \right) \left(-u^b u^c + d^b d^c \right)$$

$$+ \; \left(u^d u^e + d^d d^e \right) \left(u^b u^c + d^b d^c \right)$$

$$- \; \left(u^d d^e + d^d u^e \right) \left(u^b d^c + d^b u^c \right) \Big]$$

$$= \; \frac{1}{2} \varepsilon^{xfa} \varepsilon^{fde} \varepsilon^{abc}$$

$$\times \; \left(2 u^d u^e d^b d^c + 2 d^d d^e u^b u^c - 4 u^d d^e u^b d^c \right) ,$$

because

$$\varepsilon^{fde} d^d S u^e = -\varepsilon^{fde} u^e S^T d^d = \varepsilon^{fde} u^d S^T d^e = \varepsilon^{fde} u^d S d^e$$

for symmetric matrices S.

Therefore,

$$M_{mnop}^{VVx} \; = \; \varepsilon^{abc} \left(\delta^{ad} \delta^{xe} - \delta^{ae} \delta^{xd} \right)$$

$$\times \; \left(u^d u^e d^b d^c + d^d d^e u^b u^c - 2 u^d d^e u^b d^c \right)$$

$$= \; \varepsilon^{abc} \big[u^a u^x d^b d^c + d^a d^x u^b u^c$$

$$- \; 2 u^a d^x u^b d^c - (x \longleftrightarrow a) \big]$$

$$= \; \varepsilon^{abc} \big[u_m^a u_n^x d_o^b d_p^c + u_o^b u_p^c d_m^a d_n^x$$

$$+ \; 2 u_m^a u_o^b d_n^x d_p^c - (x \longleftrightarrow a) \big].$$

Finally, we have the following expression:

$$\left\langle M^{VV} \times \overline{M^{VV}} \right\rangle = \varepsilon^{abc}\varepsilon^{ABC}$$

$$\times \ \left[{}^{axAX}_{mnMN} \cdot {}^{bcBC}_{opOP} + {}^{axBC}_{mnOP} \cdot {}^{bcAX}_{opMN} + 2 \cdot {}^{axAB}_{mnMO} \cdot {}^{bcXC}_{opNP} \right.$$

$$+ \quad {}^{bcAX}_{opMN} \cdot {}^{axBC}_{mnOP} + {}^{bcBC}_{opOP} \cdot {}^{axAX}_{mnMN} + 2 \cdot {}^{bcAB}_{opMO} \cdot {}^{axXC}_{mnNP}$$

$$+ \quad 2 \cdot {}^{abAX}_{moMN} \cdot {}^{xcBC}_{npOP} + 2 \cdot {}^{abBC}_{moOP} \cdot {}^{xcAX}_{npMN}$$

$$+ \quad 4 \cdot {}^{abAB}_{moMO} \cdot {}^{xcXC}_{npNP} \pm \left(x \longleftrightarrow a, X \longleftrightarrow A \right) \Big]. \tag{5.9}$$

This expression has the same symmetries (5.5), (5.6), and (5.7) as that of SS expression (5.2). It is not so obvious as in the SS case, so we demonstrate this explicitly. Formula (5.9) can be rewritten as follows:

$$\left\langle M^{VV} \times \overline{M^{VV}} \right\rangle = 2\varepsilon^{abc}\varepsilon^{xaf}\varepsilon^{def}\varepsilon^{ABC}\varepsilon^{XAF}\varepsilon^{DEF}$$

$$\times \ \left({}^{edED}_{mnMN} \cdot {}^{bcBC}_{opOP} + {}^{edBC}_{mnOP} \cdot {}^{bcED}_{opMN} + {}^{edEB}_{mnMO} \cdot {}^{bcDC}_{opNP} \right.$$

$$+ \quad {}^{bcEB}_{opMO} \cdot {}^{edDC}_{mnNP} + {}^{ebED}_{moMN} \cdot {}^{dcBC}_{npOP} + {}^{ebBC}_{moOP} \cdot {}^{dcED}_{npMN}$$

$$+ \quad 2 \cdot {}^{ebEB}_{moMO} \cdot {}^{dcDC}_{npNP} \Big). \tag{5.10}$$

Under transformation (5.5) this expression goes to

$$\left\langle M^{VV} \times \overline{M^{VV}} \right\rangle \longrightarrow 2\varepsilon^{abc}\varepsilon^{xaf}\varepsilon^{def}\varepsilon^{ABC}\varepsilon^{XAF}\varepsilon^{DEF}$$

$$\times \ \left({}^{edED}_{opMN} \cdot {}^{bcBC}_{mnOP} + {}^{edBC}_{opOP} \cdot {}^{bcED}_{mnMN} + {}^{edEB}_{opMO} \cdot {}^{bcDC}_{mnNP} \right.$$

$$+ \quad {}^{bcEB}_{mnMO} \cdot {}^{edDC}_{opNP} + {}^{ebED}_{omMN} \cdot {}^{dcBC}_{pnOP} + {}^{ebBC}_{omOP} \cdot {}^{dcED}_{pnMN}$$

$$+ \quad 2 \cdot {}^{ebEB}_{omMO} \cdot {}^{dcDC}_{pnNP} \Big) \equiv 2\varepsilon^{aed}\varepsilon^{xaf}\varepsilon^{cbf}\varepsilon^{ABC}\varepsilon^{XAF}\varepsilon^{DEF}$$

$$\times \ \left({}^{bcED}_{opMN} \cdot {}^{edBC}_{mnOP} + {}^{bcBC}_{opOP} \cdot {}^{edED}_{mnMN} + {}^{bcEB}_{opMO} \cdot {}^{edDC}_{mnNP} \right.$$

$$+ \quad {}^{edEB}_{mnMO} \cdot {}^{bcDC}_{opNP} + {}^{beED}_{omMN} \cdot {}^{cdBC}_{pnOP} + {}^{beBC}_{omOP} \cdot {}^{cdED}_{pnMN}$$

$$+ \quad 2 \cdot {}^{beEB}_{omMO} \cdot {}^{cdDC}_{pnNP} \Big) \equiv - \left\langle M^{VV} \times \overline{M^{VV}} \right\rangle.$$

Under transformation (5.6) expression (5.10) goes to

$$\left\langle M^{VV} \times \overline{M^{VV}} \right\rangle \longrightarrow 2\varepsilon^{abc}\varepsilon^{xaf}\varepsilon^{def}\varepsilon^{ABC}\varepsilon^{XAF}\varepsilon^{DEF}$$

$$\times \left({}^{edED}_{mnOP} \cdot {}^{bcBC}_{opMN} + {}^{edBC}_{mnMN} \cdot {}^{bcED}_{opOP} + {}^{edEB}_{mnOM} \cdot {}^{bcDC}_{opPN} \right.$$

$$+ \ {}^{bcEB}_{opOM} \cdot {}^{edDC}_{mnPN} + {}^{ebED}_{moOP} \cdot {}^{dcBC}_{npMN} + {}^{ebBC}_{moMN} \cdot {}^{dcED}_{npOP}$$

$$+ \ 2 \cdot {}^{ebEB}_{moOM} \cdot {}^{dcDC}_{npPN} \right) \equiv 2\varepsilon^{abc}\varepsilon^{xaf}\varepsilon^{def}\varepsilon^{AED}\varepsilon^{XAF}\varepsilon^{CBF}$$

$$\times \left({}^{edBC}_{mnOP} \cdot {}^{bcED}_{opMN} + {}^{edED}_{mnMN} \cdot {}^{bcBC}_{opOP} + {}^{edBE}_{mnOM} \cdot {}^{bcCD}_{opPN} \right.$$

$$+ \ {}^{bcBE}_{opOM} \cdot {}^{edCD}_{mnPN} + {}^{ebBC}_{moOP} \cdot {}^{dcED}_{npMN} + {}^{ebED}_{moMN} \cdot {}^{dcBC}_{npOP}$$

$$+ \ 2 \cdot {}^{ebBE}_{moOM} \cdot {}^{dcCD}_{npPN} \right) \equiv - \left\langle M^{VV} \times \overline{M^{VV}} \right\rangle.$$

Finally, under transformation (5.7) expression (5.10) goes to

$$\left\langle M^{VV} \times \overline{M^{VV}} \right\rangle \longrightarrow 2\varepsilon^{abc}\varepsilon^{xaf}\varepsilon^{def}\varepsilon^{ABC}\varepsilon^{XAF}\varepsilon^{DEF}$$

$$\times \left({}^{edED}_{nmNM} \cdot {}^{bcBC}_{poPO} + {}^{edBC}_{nmPO} \cdot {}^{bcED}_{poNM} + {}^{edEB}_{nmNP} \cdot {}^{bcDC}_{poMO} \right.$$

$$+ \ {}^{bcEB}_{poNP} \cdot {}^{edDC}_{nmMO} + {}^{ebED}_{npNM} \cdot {}^{dcBC}_{moPO} + {}^{ebBC}_{npPO} \cdot {}^{dcED}_{moNM}$$

$$+ \ 2 \cdot {}^{ebEB}_{npNP} \cdot {}^{dcDC}_{moMO} \right) \equiv 2\varepsilon^{acb}\varepsilon^{xaf}\varepsilon^{edf}\varepsilon^{ACB}\varepsilon^{XAF}\varepsilon^{EDF}$$

$$\times \left({}^{deDE}_{nmNM} \cdot {}^{cbCB}_{poPO} + {}^{deCB}_{nmPO} \cdot {}^{cbDE}_{poNM} + {}^{deDC}_{nmNP} \cdot {}^{cbEB}_{poMO} \right.$$

$$+ \ {}^{cbDC}_{poNP} \cdot {}^{deEB}_{nmMO} + {}^{dcDE}_{npNM} \cdot {}^{ebCB}_{moPO} + {}^{dcCB}_{npPO} \cdot {}^{ebDE}_{moNM}$$

$$+ \ 2 \cdot {}^{dcDC}_{npNP} \cdot {}^{ebEB}_{moMO} \right) \equiv \left\langle M^{VV} \times \overline{M^{VV}} \right\rangle.$$

We notice that the last term of expression (5.10) gives us the corresponding expression for the SS block. We use this fact to store the result of calculating this last term to calculate the SS block.

5.3 SV and VS blocks

To get expressions for the SV and VS cases, we proceed analogously to the above derivations. They also have the same three symmetries. Just like in the SS case, the expressions are given by a few terms of expression (5.10), and so in the process

of calculating the VV block, we just store those terms to construct the SV and VS blocks later.

Chapter 6

Lattice results

6.1   Nucleons and kaons

The lowest kaon and nucleon masses (at zero momentum) in each channel are given in Tab. 6.1. In the negative-parity sector, only G_{1g} (corresponding to spin $\frac{1}{2}^+$ in the continuum) and A_{1u}^+ and T_{1u}^- (0^{-+} and 1^{--}) can give scattering states with energies within $0.3\,a^{-1}$ of threshold. We have also computed energies of states with finite momentum for these spins. They are given in Tab. 6.2. By adding nucleon and kaon energies, we obtain the predictions of energies of scattering states in Tab. 6.3. The true energies will be modified by interactions, of course. Figure 6-1 shows all these energies for the case of degenerate quark masses, together with energies computed from the masses in the larger volume using the continuum dispersion relation for negative parity.

In Fig. 6-2 we plot the analogous sums for the positive-parity sector.

6.2   Scattering operators

We start with lattice results for scattering operators here and then will proceed to local operators, since the former are naturally connected to the nucleons and kaons. For negative parity, we have four interpolating operators (2.102-2.105), while for positive parity we use six operators (2.106-2.111). Thus, we are diagonalizing 4×4 and 6×6

Table 6.1: Masses of nucleons and kaons at rest. Charge-conjugation labels apply to the cases with $m_q = m_s$ only.

particle	$^2O_h^-$ rep.	$16^3 \cdot 64$ $m_q = m_s$	$24^3 \cdot 64$ $m_q = m_s$	$24^3 \cdot 64$ $m_q < m_s$	cont. spin
N	G_{1g}	0.7966(17)	0.791(2)	0.570(3)	$\frac{1}{2}^+$
		1.263(15)	1.263(13)	1.12(5)	
	G_{1u}	1.044(6)	1.047(7)	0.88(3)	$\frac{1}{2}^-$
	H_g	1.257(13)	1.279(12)	1.12(3)	$\frac{3}{2}^+$
	H_u	1.053(7)	1.070(6)	0.91(2)	$\frac{3}{2}^-$
K	A_{1u}^+	0.4219(3)	0.4217(4)	0.3388(4)	0^{-+}
		0.847(28)	0.919(18)	0.88(4)	
	A_{1g}^+	0.742(5)	0.735(6)	0.693(9)	0^{++}
	A_{1g}^-	1.07(6)	1.16(6)		0^{+-}
	T_{1u}^-	0.5055(7)	0.5060(8)	0.4489(10)	1^{--}
		0.953(29)	0.984(16)	0.94(2)	
	T_{1g}^+	0.767(5)	0.777(4)	0.732(7)	1^{++}
	T_{1g}^-	0.772(7)	0.778(7)		1^{+-}

Table 6.2: Energies of nucleons and kaons with momentum, where $p_0 = 2\pi/L$ denotes the lowest non-zero momentum on the periodic lattice.

	$\vec{p}$	lattice rep.	$16^3 \cdot 64$ $m_q = m_s$	$24^3 \cdot 64$ $m_q = m_s$	$24^3 \cdot 64$ $m_q < m_s$	cont. hel.
N	$(0,0,p_0)$	E_1	0.8832(24)	0.8309(24)	0.629(4)	$\frac{1}{2}$
	$(0,p_0,p_0)$	E	0.9618(47)	0.8691(33)	0.682(5)	$\frac{1}{2}$
K	$(0,0,p_0)$	A_2^+	0.5726(19)	0.4946(9)	0.4275(12)	0^{-+}
	$(0,0,p_0)$	A_1^-	0.6323(19)	0.5681(12)	0.5187(16)	0^{+-}
	$(0,0,p_0)$	E_2^-	0.6327(20)	0.5682(12)	0.5190(16)	1^-
	$(0,p_0,p_0)$	A_2^+	0.678(10)	0.5582(22)	0.4997(35)	0^{-+}
	$(0,p_0,p_0)$	A_1^-	0.746(4)	0.6206(24)	0.5753(35)	0^{+-}
	$(0,p_0,p_0)$	B_1^-	0.744(5)	0.6229(26)	0.5777(35)	1^-
	$(0,p_0,p_0)$	B_2^-	0.748(5)	0.6228(26)	0.5783(36)	1^-

Table 6.3: Sums of nucleon and kaon energies with negative total parity.

$\vec{p}$	N	K	$16^3 \cdot 64$ $m_q = m_s$	$24^3 \cdot 64$ $m_q = m_s$	$24^3 \cdot 64$ $m_q < m_s$	cont. reps.
$(0,0,0)$	G_{1g}	A_{1u}^+	1.2185(18)	1.2126(19)	0.909(3)	$\frac{1}{2}^+$ 0^{-+}
$(0,0,0)$	G_{1g}	T_{1u}^-	1.3021(20)	1.2969(23)	1.019(4)	$\frac{1}{2}^+$ 1^{--}
$(0,0,p_0)$	E_1	A_2^+	1.4558(39)	1.3254(28)	1.056(5)	$\frac{1}{2}$ 0^{-+}
$(0,0,p_0)$	E_1	A_1^-	1.5155(38)	1.3989(31)	1.147(5)	$\frac{1}{2}$ 0^{+-}
$(0,0,p_0)$	E_1	E_2^-	1.5159(39)	1.3990(30)	1.148(5)	$\frac{1}{2}$ 1^-
$(0,p_0,p_0)$	E	A_2^+	1.640(13)	1.4272(50)	1.182(8)	$\frac{1}{2}$ 0^{-+}
$(0,p_0,p_0)$	E	A_1^-	1.708(7)	1.4897(53)	1.257(8)	$\frac{1}{2}$ 0^{+-}
$(0,p_0,p_0)$	E	B_1^-	1.706(8)	1.4920(55)	1.260(8)	$\frac{1}{2}$ 1^-
$(0,p_0,p_0)$	E	B_2^-	1.709(8)	1.4919(56)	1.260(8)	$\frac{1}{2}$ 1^-
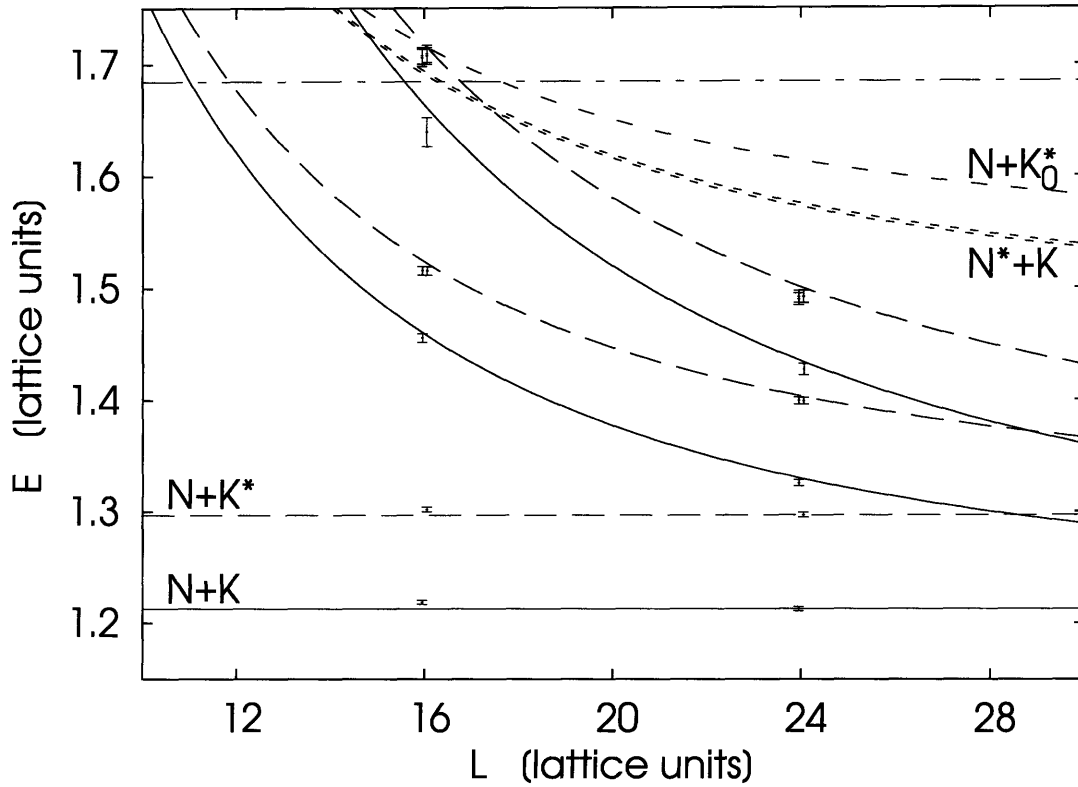
Figure 6-1: Sums of nucleon and kaon energies with negative total parity. Different relative momenta have the same line type for the same constituent hadrons.
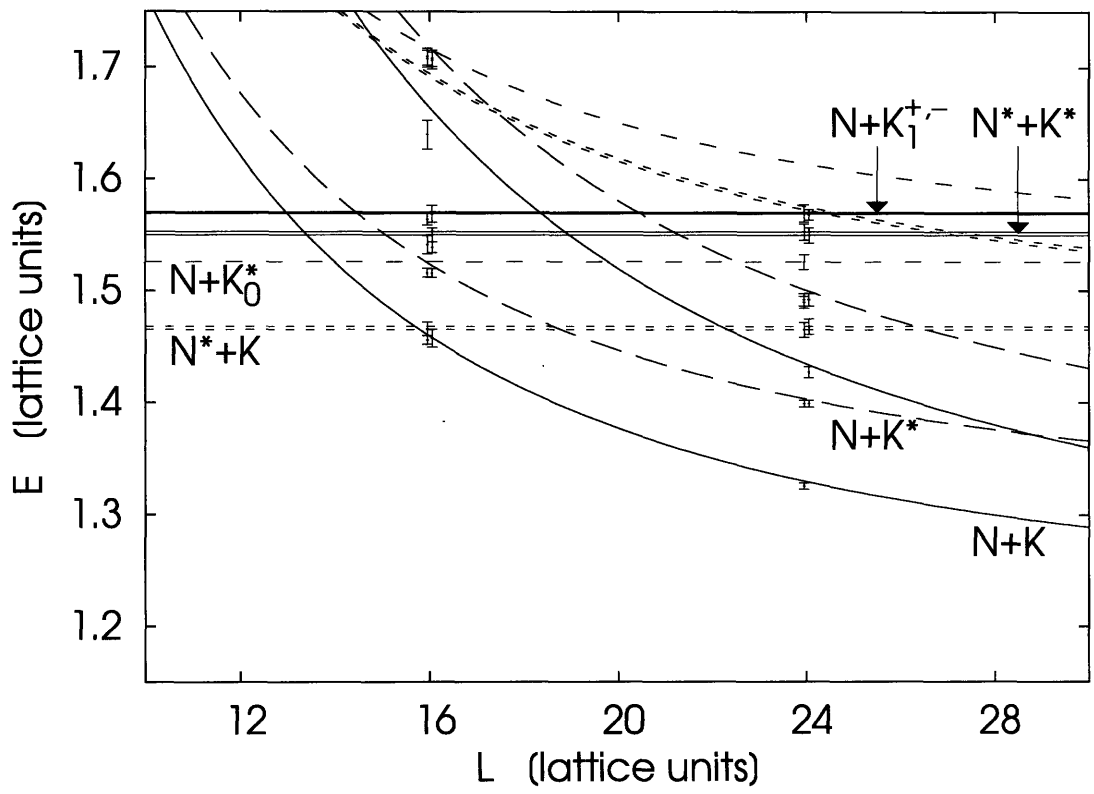
Figure 6-2: Sums of nucleon and kaon energies with positive total parity. Notation is the same as in Fig. 6-1.

correlation matrices. We always count time from the source so that $t_{src} = 0$ by convention. The Dirichlet boundary is thus at $t = -11$. For the sake of convenience, as well as for comparison with other works, we always use effective mass to present measurements of eigenvalues of correlation matrices.

Effective mass is defined as follows:

$$M_{\text{eff}}(t) = \log \frac{\lambda(t - 1/2)}{\lambda(t + 1/2)},$$ (6.1)

where t is in lattice units. Since an eigenvalue on the lattice is only defined in integer points, t in the above expression has to be half-integer: $\pm 1/2, \pm 3/2$, and so on. Note that our definition is different from the one used in many other works, where it is such that effective mass also takes an integer argument. We emphasized symmetry over convenience: a point on our graph immediately shows which two time slices the underlying eigenvalues belong to.

Substituting the asymptotic expression for an eigenvalue

$$\lambda(t) \to \exp(-Et) \ \text{ as } \ t \to \infty,$$ (6.2)

we get $M_{\text{eff}}(t) \to E$ as $t \to \infty$. This is the reason for introducing the concept of effective mass: as we go to larger times, our signal converges to the energy we are measuring. Plotting effective mass for a range of times gives us a means of assessing the quality of the signal visually.

Technical methods used in literature for extracting energy E from an effective mass plot vary. The simplest method is fitting it with a constant in some range $[t_a, t_b]$, where t_a is chosen large enough so that the approximation (6.2) is valid, while t_b must be far enough from the boundary so as to minimize boundary effects.

On good signals, usually for low-lying states, we use an equivalent variation of this method. We fit the underlying eigenvalue directly with an exponential. However, choosing values t_a and t_b is an art rather than science—albeit the resulting energy is insensitive to the choice provided the signal is good enough. We do always show them by plotting the resulting errorband that starts at t_a and ends at t_b.

This method only works on good signals and good plateaus. Unfortunately, in this work we often step in the territory where we are unable to obtain good plateaus despite the enormous statistics. In such cases, fitting with something more elaborate than a constant is desirable.

Motivated by the fact that the correlation function can be expressed as a super-composition of decaying exponentials, we fit the underlying eigenvalues directly with the truncated sum

$$f(t, A, m, A_1, m_1) = A \exp(-mt) + A_1 \exp(-m_1 t). \tag{6.3}$$

We enforce the condition $m_1 > m$, so that (6.3) approaches the lowest state for large enough t. We are still required to specify the fitting range $[t_a, t_b]$ by hand.

In the case of a 1×1 correlation matrix, its only eigenvalue is also a correlation function, so that it is a sum of the form

$$\text{c.f.}(t) = \sum_i A_i \exp(-E_i t), \tag{6.4}$$

where E_i are the energies in the energy spectrum, while A_i are overlaps of the interpolating operator with the state corresponding to energies E_i. Our fitting function is just the first two terms in the sum.

This picture scales to the general case of an $N \times N$ correlation matrix when the eigenvectors are independent of t, as its eigenvalues are then correlation functions. The fitting function works well in practice, and we employ it wherever we do not have a good enough plateau.

6.2.1 Negative parity

Fig. 6-3 and 6-5 show the eigenvalues of the 4×4 negative parity correlation matrix on two volumes. On the same plots, we show the relevant sums of kaon and nucleon energies from Tab. 6.3—also plotted in Fig. 6-1. Our interpolating operators (2.102-2.105) are constructed with the goal of having a good overlap with four lowest-lying
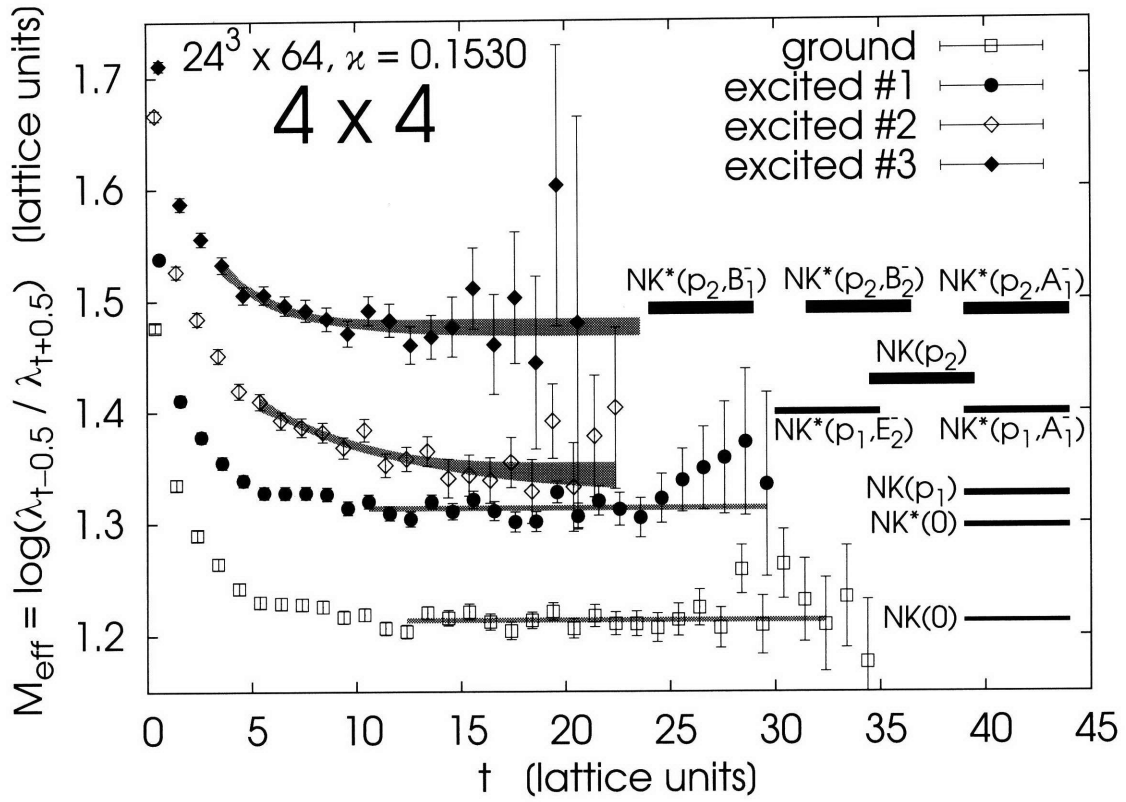
Figure 6-3: Effective masses of eigenvalues for scattering operators with fits and sums of single-particle energies for a $24^3 \times 64$ lattice with $m_q = m_s$ and negative parity. $p_1 = (0, 0, p_0)$, $p_2 = (0, p_0, p_0)$, where $p_0 = 2\pi/L$.
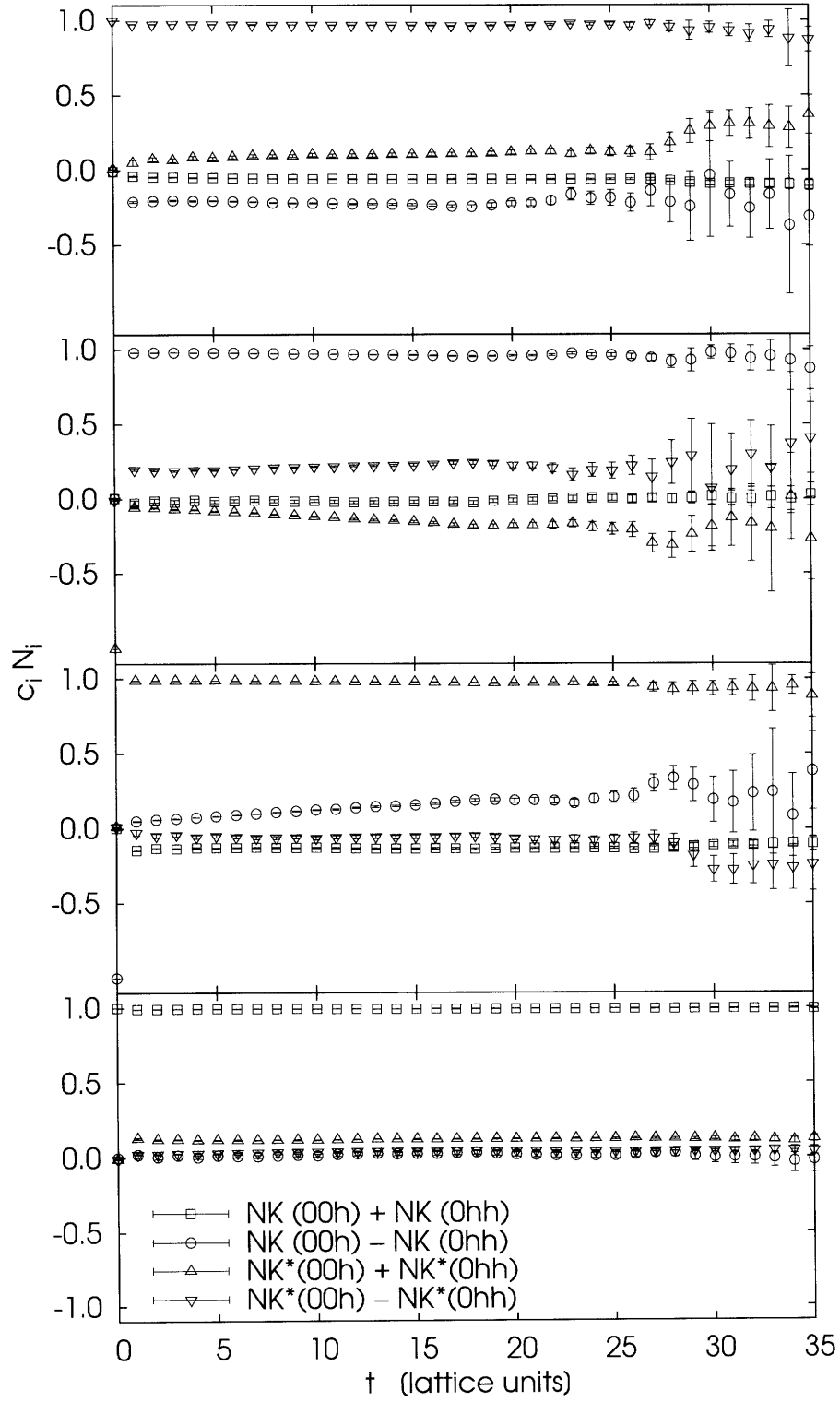
Figure 6-4: Eigenvectors normalized by true norms N_i for a $24^3 \times 64$ lattice with $m_q = m_s$ and negative parity.
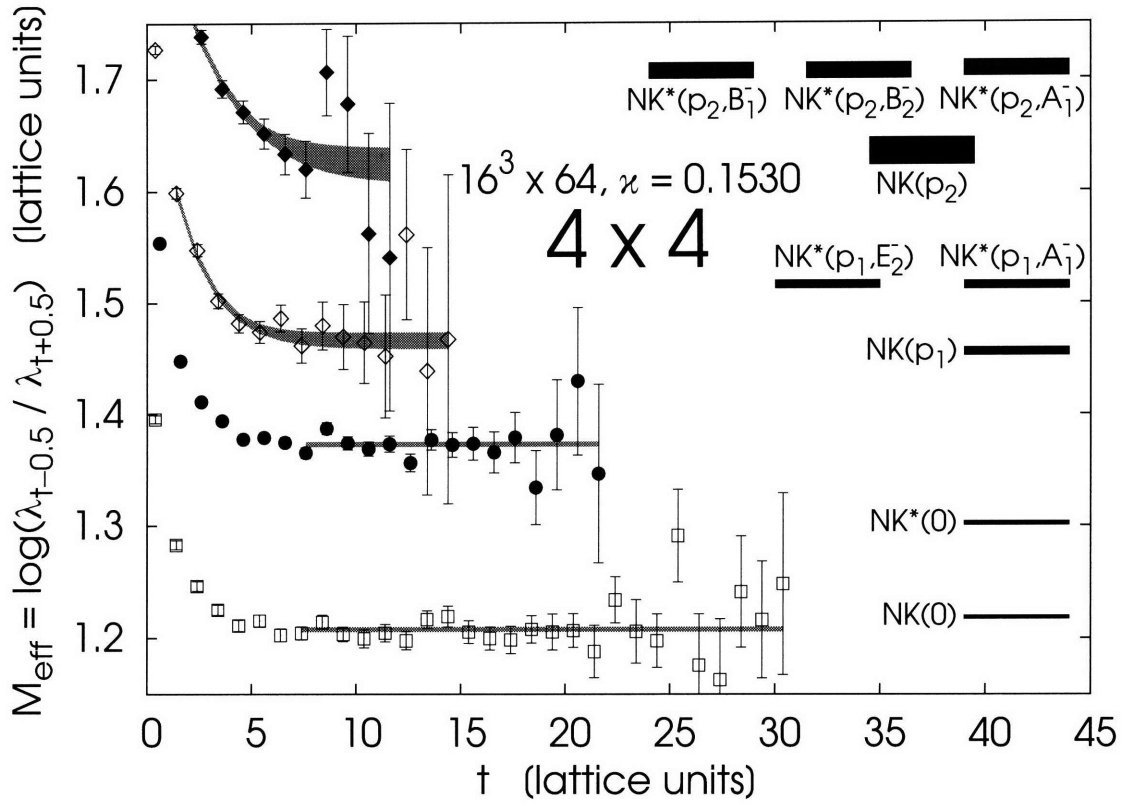
Figure 6-5: Effective masses of eigenvalues for scattering operators with fits and sums of single-particle energies for a $16^3 \times 64$ lattice with $m_q = m_s$ and negative parity. $p_1 = (0, 0, p_0)$, $p_2 = (0, p_0, p_0)$, where $p_0 = 2\pi/L$.
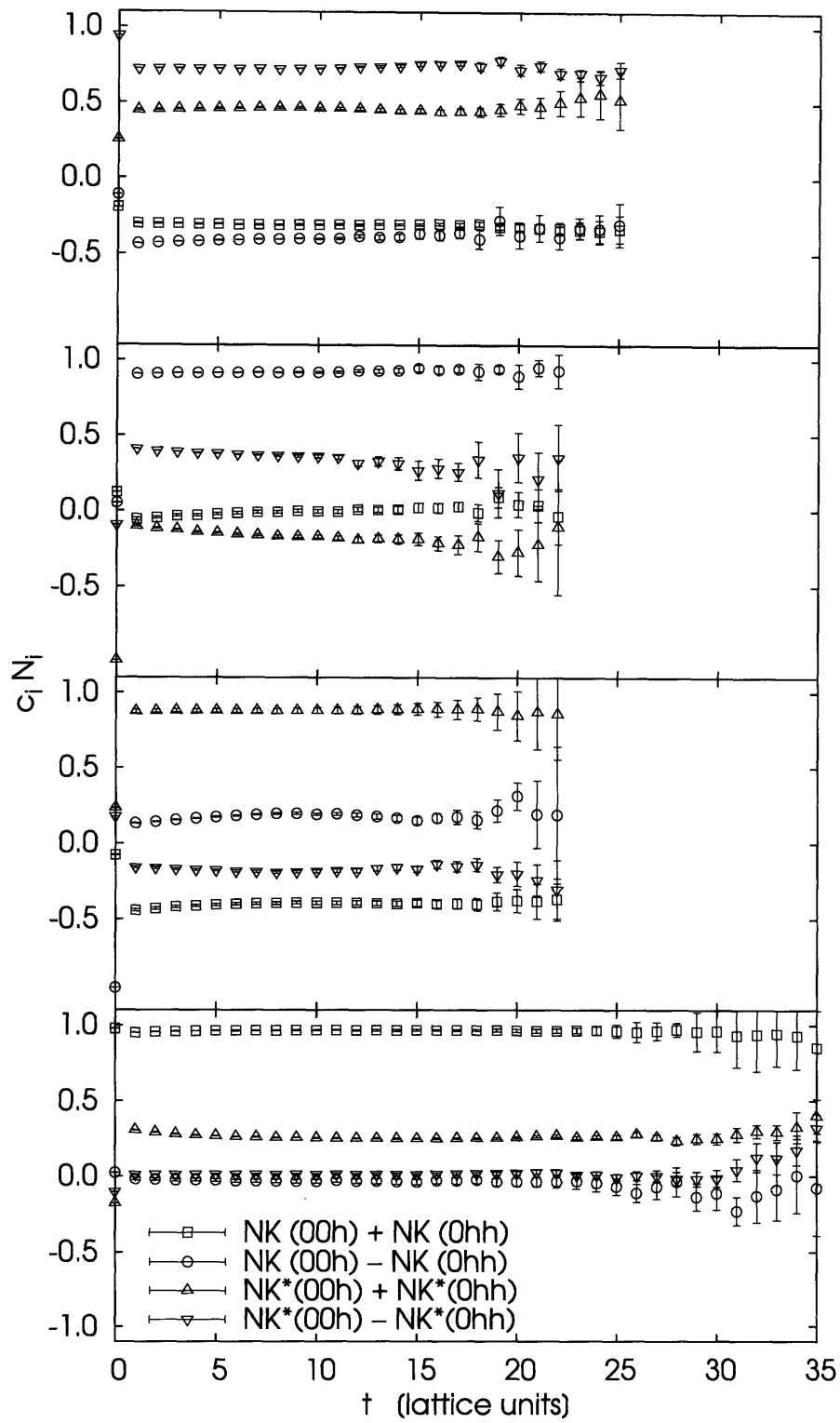
Figure 6-6: Eigenvectors normalized by true norms N_i for a $16^3 \times 64$ lattice with $m_q = m_s$ and negative parity.

states. We see in the larger-volume figure 6-3 that the first three eigenvalues are close to the first three sums of kaon and nucleon energies, although only the first and third agree within statistical errors. The two sources involving K^* have a worse agreement, while the K sources agree beautifully.

As explained above, we fit the two lowest-lying eigenvalues with a single exponential. We employ our two-exponential fit (6.3) for the remaining two eigenvalues as they do not have very good plateaus. The resulting errorbars are shown on the plots.

We expect our correlation matrix to be nearly diagonal, since our interpolating operators have good overlaps with their own energy states and bad overlaps with other states. Fig. 6-4 and 6-6 show the actual measurements of expansion coefficients as functions of t. The correlation matrix is indeed nearly diagonal except on the smaller volume with the highest state, where we observe strong mixing. Note that statistical noise begins to set in at $t \approx 25$ for excited states on the 24^3 lattice and the ground state on the 16^3 lattice, and at $t \approx 15$ for excited states on the 16^3 lattice.

6.2.2   Positive parity

We now proceed to the correlation matrix of the six operators (2.106-2.111) tailored to positive parity. Unlike for negative parity, we only show results on the larger volume here. Fig. 6-7 shows the eigenvalues of the 6×6 positive parity correlation matrix with the relevant sums of kaon and nucleon energies from Tab. 6.3. They were plotted in Fig. 6-2. Note that the spectrum is much more dense for positive parity compared to the analogous case for negative parity. We can only clearly associate the lowest measured scattering state with the lowest kaon-nucleon energy sum. The next three states clearly do not agree within errorbars, although we could probably say that the fourth state ought to be $NK(p_2)$, as all other candidates are either taken or lie noticeably higher. Another thing we can say is that our operators do not capture the two N^*K states, since there is clearly a gap in the measured spectrum where these states are supposed to be.

Note that we use two-exponential fits (6.3) for all six states in this case because the signal is not as good as for negative parity, leading to a somewhat worse quality
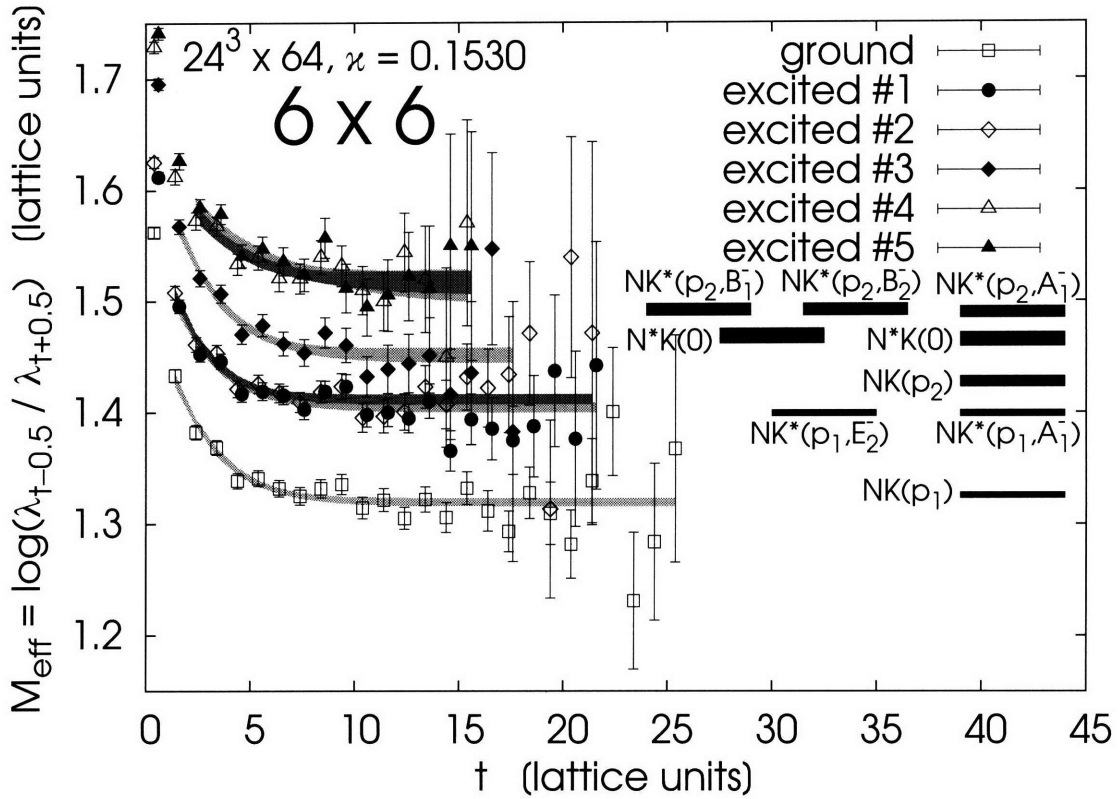
Figure 6-7: Effective masses of eigenvalues for scattering operators with fits and sums of single-particle energies for a $24^3 \times 64$ lattice with $m_q = m_s$ and positive parity. $p_1 = (0, 0, p_0)$, $p_2 = (0, p_0, p_0)$, where $p_0 = 2\pi/L$.
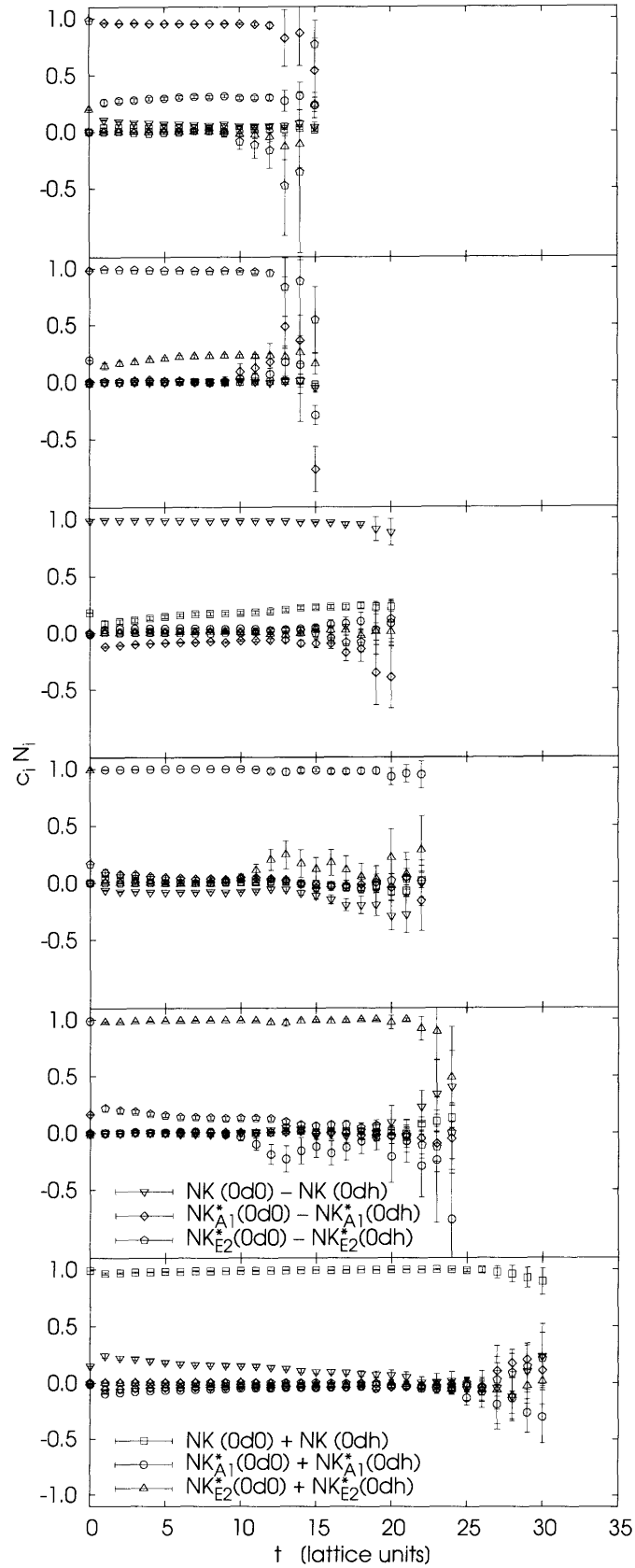
Figure 6-8: Eigenvectors normalized by true norms N_i for a $24^3 \times 64$ lattice with $m_q = m_s$ and positive parity.

of the plateaus.

Of course, the picture clarifies once we look at the measurement of expansion coefficients.

Analogously to the negative parity case, the six operators were designed to have good overlaps with certain energy states and bad ones with everything else. The correlation matrix is remarkably close to being diagonal here, as shown in Fig. 6-8. With the help of this plot we confirm the observations made while looking at the effective mass plot.

The sequence of states in the measured spectrum is as follows, low to high:

$$NK(p_1), NK^*(p_1, E_2^-), NK^*(p_1, A_1^-), NK(p_2), NK^*(p_2, E_2^-), NK^*(p_2, A_1^-).$$

Interestingly, E_2^- states are lower than A_1^- states in the measured spectrum and higher in the sums of kaon and nucleon energies.

6.3   Local operators

We now proceed to lattice measurements for the nineteen local interpolating operators. Analogously to the scattering results, we start with eigenvalues and then move on to the corresponding eigenvectors, or expansion coefficients. Since we have many correlation matrices here, the results pertaining to expansion coefficients are moved to a separate chapter. In this chapter, we concentrate on the analysis of correlation matrices. We would like to carefully annotate what a particular correlation matrix brings to the table, and at what cost, computational or otherwise. We consider two different bases of local interpolating operators, but the difference between them is left for the expansion coefficient section because correlation matrices are clearly independent of the basis.

Fig. 6-9 shows the result of diagonalizing the 19×19 correlation matrix on two volumes, and two light quark masses on the larger volume. Again we set $t = 0$ at the source, and the Dirichlet boundary is at $t = -11$ with this convention. Effective mass

depends on two adjacent temporal points, and so we assign its value to the average of those points, so that, for example, $M_{eff}(t = 1/2)$ depends on correlation functions $C(t = 0)$ and $C(t = 1)$.

Gray errorbands on the plots correspond to two-exponential fits of the eigenvalues. As for most cases for scattering operators, the fitting function (6.3) is employed. Note that eigenvalues themselves, not effective masses, are fitted. At large t, the errorbands show the value and error of fit parameter m that yields a particular energy level.

We compare our energy levels to those given by the three commonly used sources: Sasaki, KN, and color-fused KN. In Fig. 6-10, we plot the signal from the three sources together with the lowest two errorbands from Fig. 6-9. This shows us that the common sources by themselves can only be used to extract the ground energy level, with KN and color-fused KN being virtually as good as the result of diagonalization. The Sasaki source apparently has much more admixture of higher-lying states, but still can hardly be used to extract information about them.

Having a 3D-rotationally covariant basis of interpolating operators, we have many options of picking elements in the basis to study other correlation matrices. We study two options. First, we consider a complete basis, but with the stronger restriction of Lorentz-covariance. This basis has 8 interpolating operators. Secondly, we construct the conventional 3×3 correlation matrix with the three commonly used sources. Note that those sources are Lorentz-covariant.

Fig. 6-11, Fig. 6-12 and Fig. 6-13 show the results of diagonalizing using the 8 and the 3 interpolating operators. Again, we plot errorbands from Fig. 6-9, the results of diagonalizing the 19×19 correlation matrix. Also, with *dark gray* we plot the results of the analogous two-exponential fits to the *shown* data. The fit to the second energy level is especially interesting. Since it shows the improvement by diagonalizing the 19×19 matrix compared to the 8×8 and 3×3 ones.

We do not have any problems extracting the ground energy level with any correlation matrix, which is no surprise since we have already seen that just one operator, say, KN, is sufficient to get the ground energy level.

As far as the first excited energy level goes, we notice two things. First, the

19×19 correlation matrix provides superior signals for this level, allowing for lower statistical errors, by a factor of up to 3. Secondly, there is a rather small difference between 8×8 and 3×3. Eigenvalues of these correlation matrices are rather close to each other. It is the 3D-rotational covariance that allows us to get a better signal. Ironically, the 8×8 correlation matrix requires just as much computer time as the 19×19 one, which is some 20 times more than the 3×3 one. The largest matrix is much harder to calculate, yet it provides slightly better signals.

We consider the possibility of improving the signals further by employing other correlation matrices. The idea is to truncate the basis of interpolating operators based on eigenvectors. Say, we are interested in extracting nth energy level as precisely as possible. We look at the elements of the corresponding eigenvector with largest moduli and only keep the interpolating operators corresponding to them. The number of the elements of the eigenvector with largest moduli is subjective and depends on the energy level.

Since we are especially interested in the ground and first excited states, we pick two sets of interpolating operators, one optimized for the ground state, the other optimized for the first excited state.

The eigenvector for the ground state is strongly dominated by 3 interpolating operators: Π_{12}, Π_{14}, and Π_{17}. Keeping the 3 and removing the other operators from the original set of 19, we obtain a new correlation matrix, $3' \times 3'$. We must not confuse it with the correlation matrix comprised of the commonly used three operators.

As for the first excited state, it has a little of almost every operator in it. We therefore select 5 eigenvectors with largest moduli: Π_1, Π_2, Π_5, Π_6, and Π_{15}.

We diagonalize the correlation matrices comprised of (a) the three, (b) the five, (c) the eight (3+5) operators. The results are plotted in Fig. 6-14. As expected, the $3' \times 3'$ matrix gives a good ground state, the $8' \times 8'$ gives first two states, while the $5' \times 5'$ gives none. Although the five operators are ideal for the first excited state, they do not allow good extraction of the ground state, so that extraction of the first excited state also fails in this case.

Surprisingly, getting rid of irrelevant operators does not improve the signal—

diagonalizing the full 19×19 matrix gives about the same signal as diagonalizing the optimized $8' \times 8'$ matrix.

6.4 Expansion coefficients

Our last "measurement" section is devoted to generalized eigenvectors, or expansion coefficients, corresponding to eigenvalues presented in the previous section. Although we have already presented eigenvectors for scattering states, we should emphasize some features of our eigenvectors that make them an especially valuable tool in exploring structure of pentaquark states.

Attempts have been made in literature to employ the naive solutions of the generalized eigenvalue problem (3.9) to make statements about structure of states. As this is a common technique in spectroscopy, the demand for their meaningful interpretation is high. Unfortunately, the attempts are largely thwarted by the lack of independence of an unphysical parameter t_0 as well as instability in t. The latter problem is alleviated by choosing $t_0 = t_{src}$. However, this choice is only possible after correct calculation of equal-time correlation function, cf. (3.3), which is practically never done in lattice calculations.

In principle, the problem of t_0-dependence exists for eigenvalues, too. We shall address it here by plotting the relative deviation of effective mass taken with various values of t_0 with respect to the $t_0 = 0$ effective mass. The results are plotted in Fig. 6-15.

We notice that the deviation is not always zero within statistical errors. However, it is only significantly different from zero when the signal has not reached a plateau yet, like in the lower-left corner of the graph which shows the result for the ground state eigenvalue taken at $t = 15$. If we go back to Fig. 6-9 where these eigenvalues are plotted, we see that the point $t = 15$ is not on the plateau yet. We have carefully checked the t_0 independence for all plateaus that we present in this work.

Things are usually much worse for eigenvectors. If we are unable to choose $t_0 = t_{src}$, we face a significant dependence on both t and t_0, including the plateau region.

This is why eigenvectors are rarely used in lattice spectroscopy despite huge incentives to do so.

This is where our two novelties come in. First, we always calculate equal-time correlation functions correctly, which gives us the freedom to choose $t_0 = t_{src}$. But more importantly, we develop a consistent definition of expansion coefficients. Our coefficients, multiplied by the corresponding interpolating operators, give an operator whose correlator is given by the eigenvalue, as it always should be with true expansion coefficients. We test the effectiveness of the t and t_0 dependence elimination process by plotting our eigenvectors as functions of t and t_0.

In Fig. 6-16, we have plotted the expansion coefficients with errorbars on the larger volume, for the degenerate quark mass. The plot shows a high degree of t-independence of expansion coefficients.

To reduce statistical errors, we fit the expansion coefficients with horizontal lines. The result of the fit for the ground state can be seen in Fig. 6-16.

Fig. 6-17 shows the success of our nearly t_0-independent definition of expansion coefficients, which have far less t_0 dependence that the naive solutions to the generalized eigenvalue problem (3.9) that are conventionally used in other works. Indeed, our coefficients are remarkably independent of t_0. There is no t_0-dependence within statistical errors for the first two states, and only mild dependence in the second excited state.

Finally, we compare our results for expansion coefficients for all volumes and masses considered in Fig. 6-18, which shows the three cases for the lowest three eigenstates, with errorbars, and sign encoded with the shade of gray. Note that the coefficients are real.

We do not show the positive parity results from the local basis of interpolating operators, since the energy spectrum there is very dense, leading to unstable correlation matrix diagonalization.

The first observation we make is that the coefficients are close to each other for all masses and volumes, indicating the very similar physical nature of the states in each case.

Secondly, for the ground state, we see three dominant operators having much bigger coefficients than the rest of the operators. These operators are the only ones that have non-zero non-relativistic limit, and in each case correspond to a nucleon plus a kaon.

Thirdly, for the first and second excited states, we conclude that we captured the same states across various volumes and masses, but cannot determine clear dominant operators for them.

To attempt to extract more information about the states from expansion coefficients, we have an alternative operator basis.

Fig. 6-19 is the analogous plot for the alternative basis. The new gem of information we learn from it concerns the ground state. Now we have indisputable evidence that the ground state is created by operator number 13 (2.53) in the alternative basis, the only one composed of only upper quark components.

Unfortunately, no new information about excited states comes from the alternative basis.
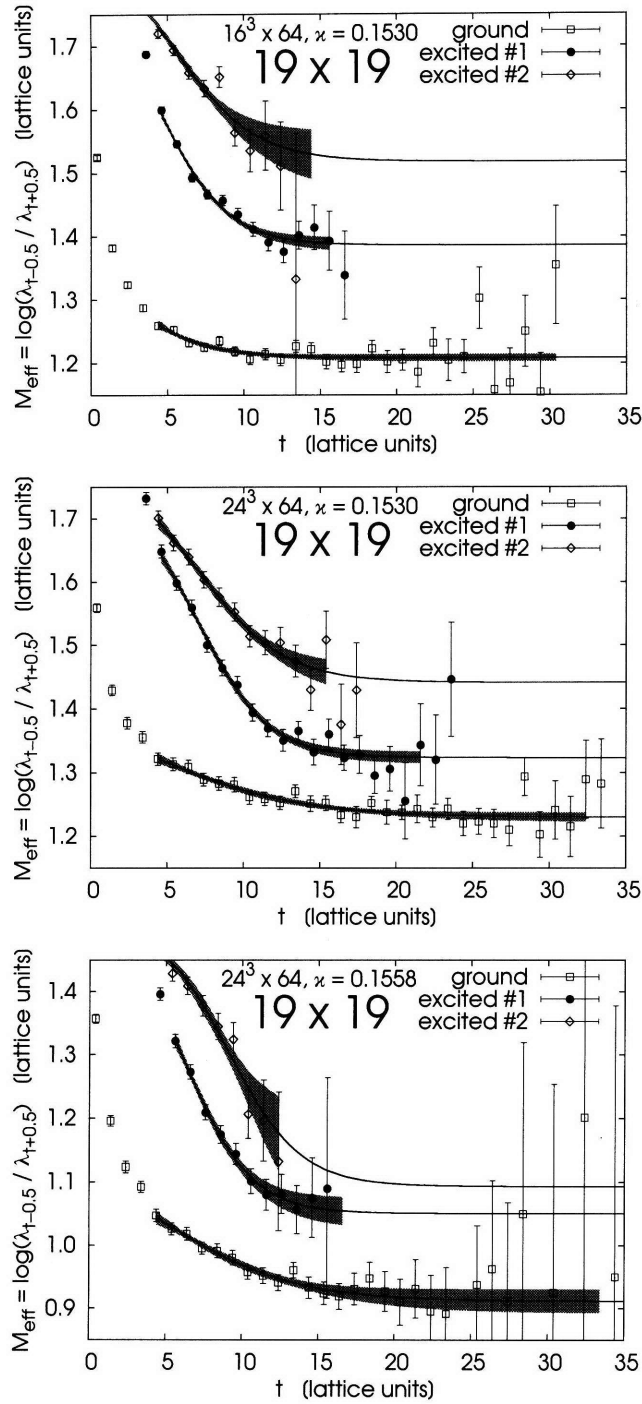
Figure 6-9: Effective masses for the lowest three negative parity eigenstates of the 19×19 correlation matrix on the $16^3 \times 64$ lattice with $\kappa_{\text{light}} = 0.1530$ and on the $24^3 \times 64$ with $\kappa_{\text{light}} = 0.1530$ and $\kappa_{\text{light}} = 0.1558$ (top to bottom).
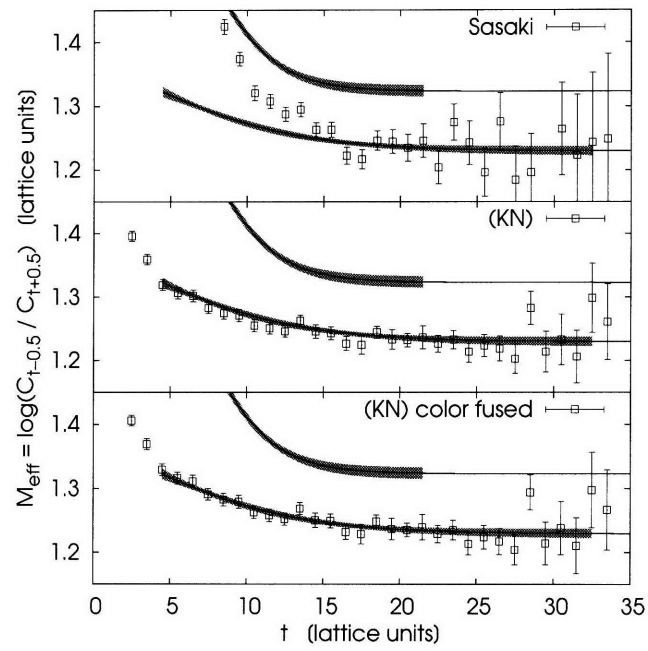
Figure 6-10: Diagonal matrix elements for three common sources on the $24^3 \times 64$ lattice with $\kappa_{\text{light}} = 0.1530$.
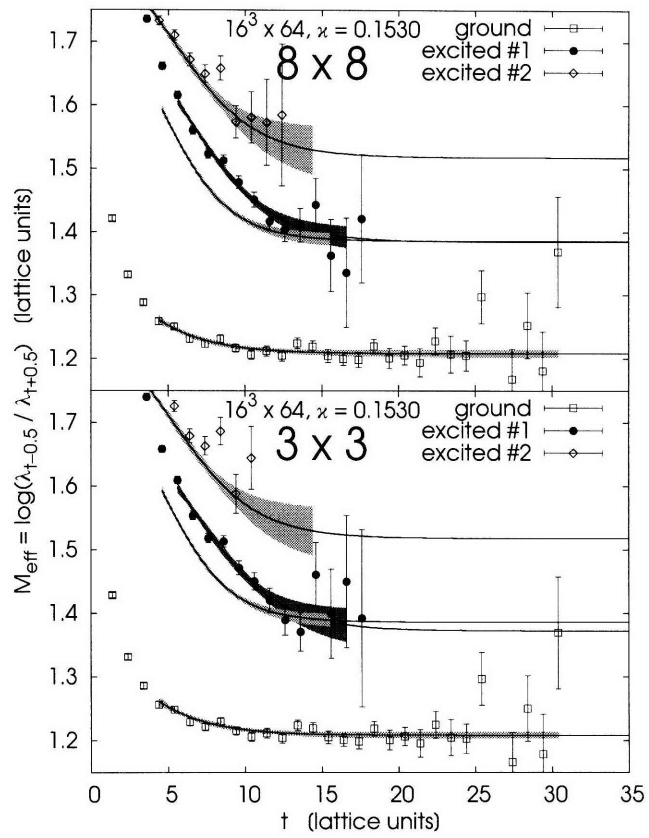
Figure 6-11: Diagonalization in two subspaces in the small volume for heavy mass.
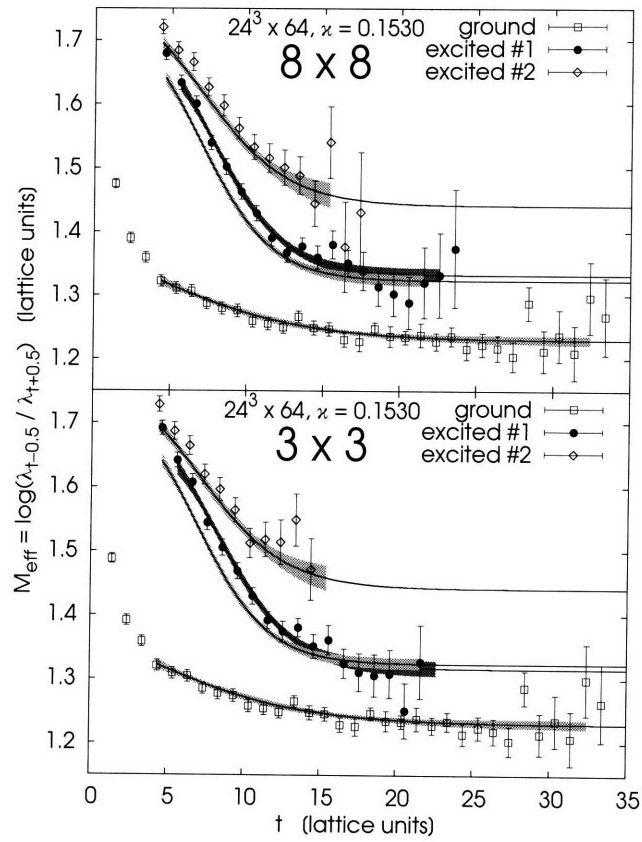
Figure 6-12: Diagonalization in two subspaces in the large volume for heavy mass.
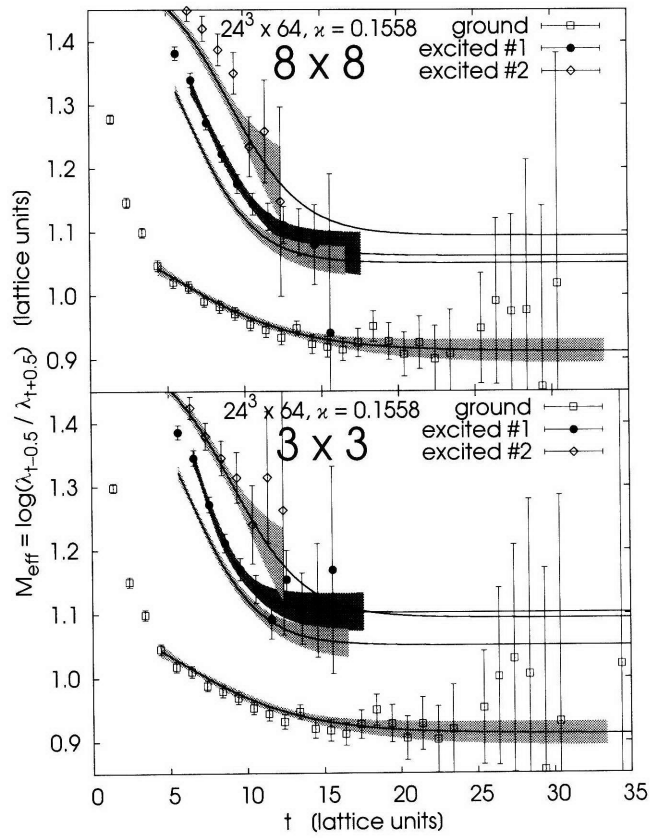
Figure 6-13: Diagonalization in two subspaces in the large volume for light mass.
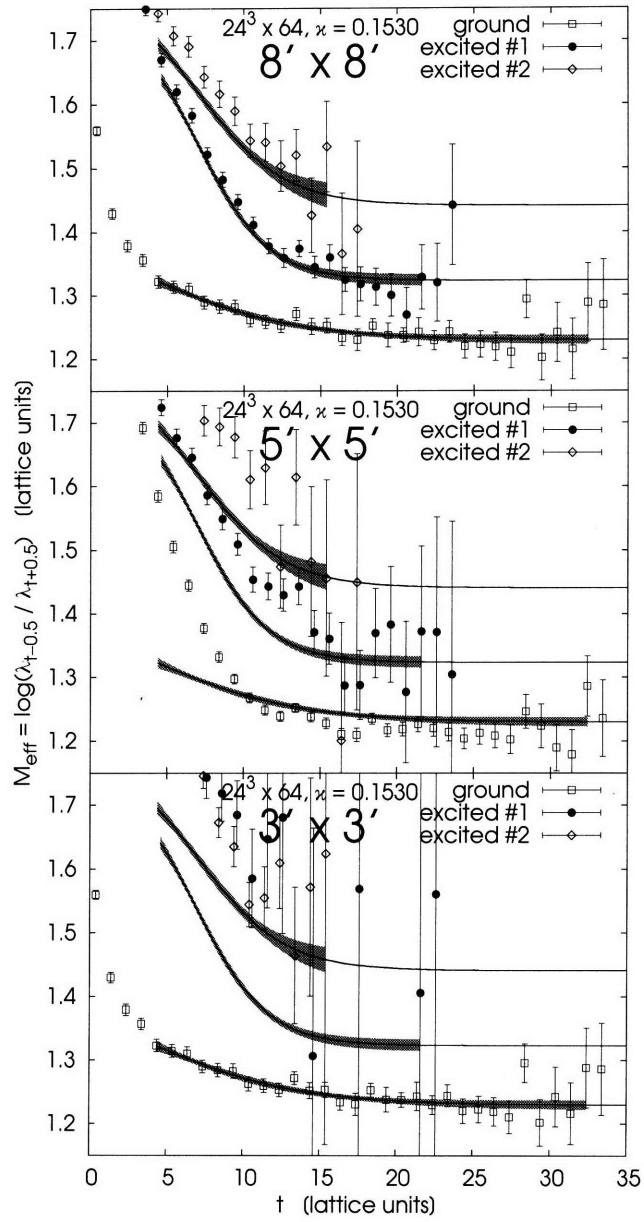
Figure 6-14: Diagonalization in the space defined by the dominant components.
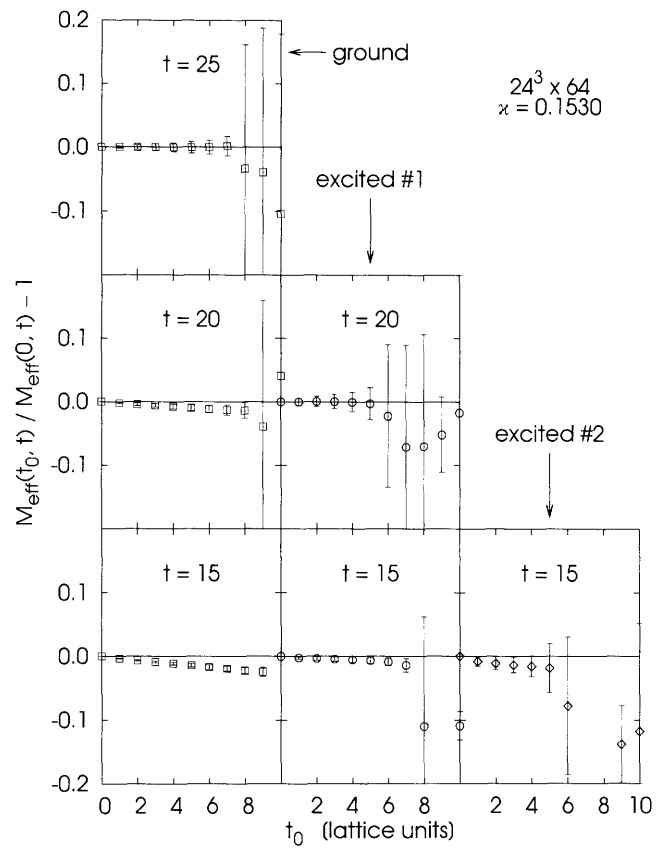
Figure 6-15: Dependence of energies on t_0.
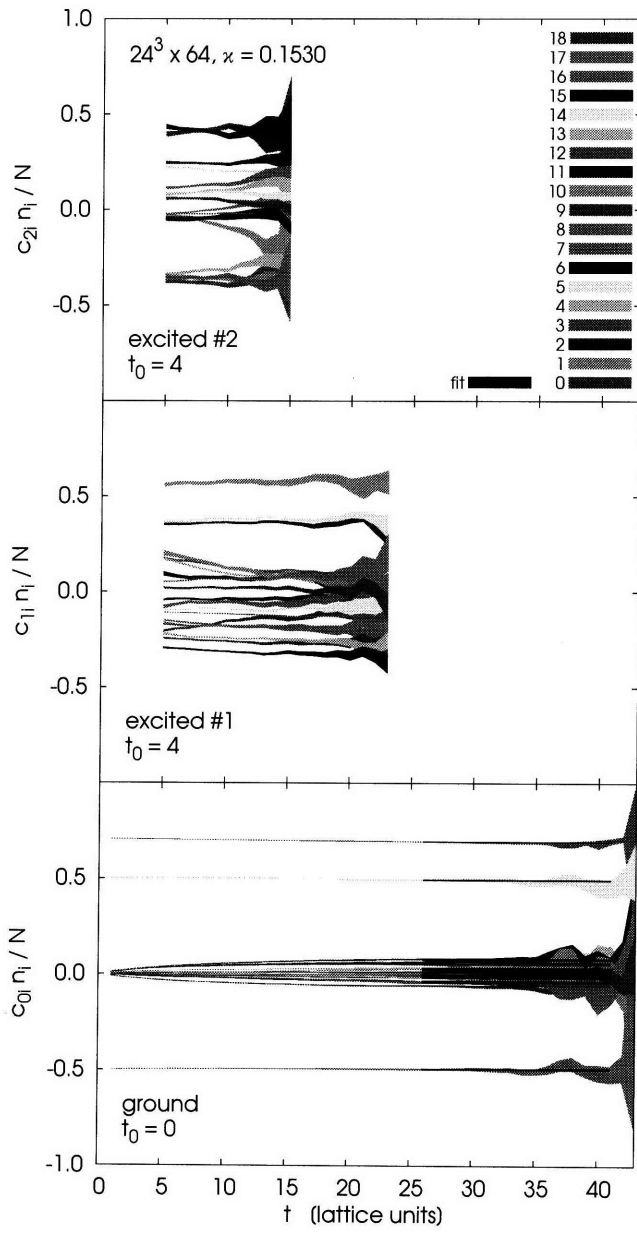
Figure 6-16: Dependence of $c_{ni}(t, t_0)$ on t for select t_0.
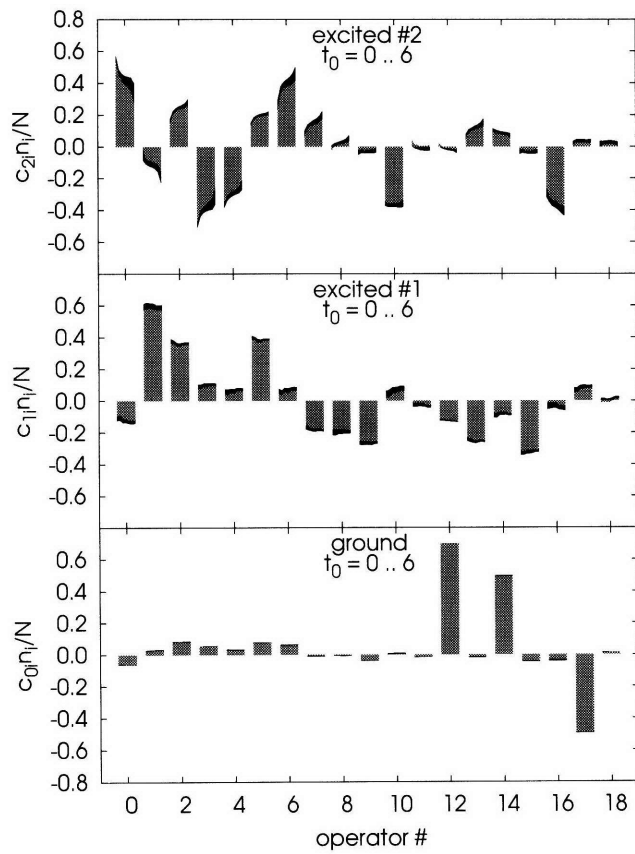
Figure 6-17: Dependence of $c_{ni}(t, t_0)$ on t_0, $24^3 \times 64$, $\kappa = 0.1530$. 7 values of the coefficients for $t_0 = 0..6$ are plotted from left to right with the error band shown in black.
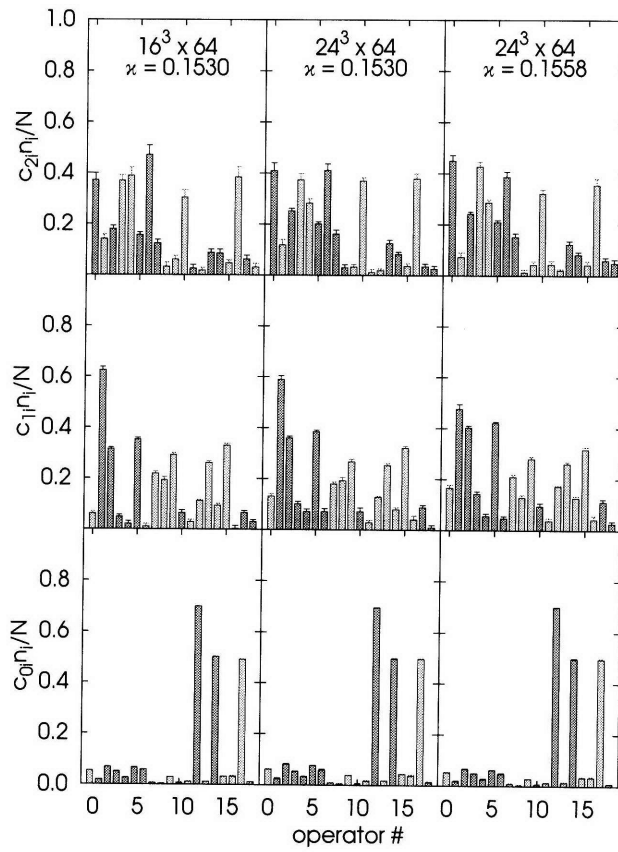
Figure 6-18: Final expansion coefficients for the lowest three eigenstates. Positive values are shown in dark gray, while negative ones are light gray.
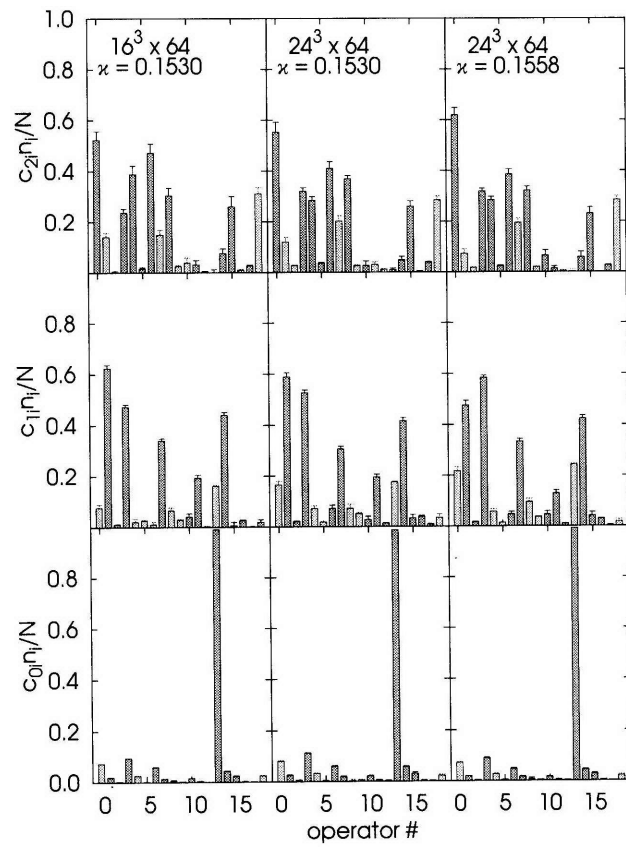
Figure 6-19: Final expansion coefficients for lowest three eigenstates: alternative basis.

Chapter 7

Summary

In this work, we have understood the physical nature of states of the low energy states of our five-quark system using a combination of local and scattering bases of interpolating operators. To summarize the arguments, we collect the relevant negative-parity results from the local and scattering bases for the heavy quark case in Fig. 7-1 showing energy measurements along with sums of nucleon and kaon energies. These results were shown in more detail in Figs. 6-3, 6-5, and 6-9. Since high density of states in the positive parity channel made discriminating among different states problematic, we are summarizing measurements in the negative parity channel only.

The ground state is measured very well with both scattering and local operators. From the local basis decomposition, we have seen a clean $K - N$ scattering state signal, since this state was dominated by the only three operators with a non-zero non-relativistic limit. The alternative local basis of operators with a definite number of upper and lower components further clarified the picture since the decomposition was dominated by one operator. In the scattering basis, we have an excellent fit and a decomposition dominated by the $K - N$ operator, confirming the observation of a $K - N$ scattering state.

The decomposition of the first excited state in the scattering basis is dominated by the $K^* - N$ operator in both volumes, and in the larger volume the energy fits agree closely with the sum of K^* and N energies as one expects for scattering states as the volume increases. The local operators yield energies slightly above but statistically
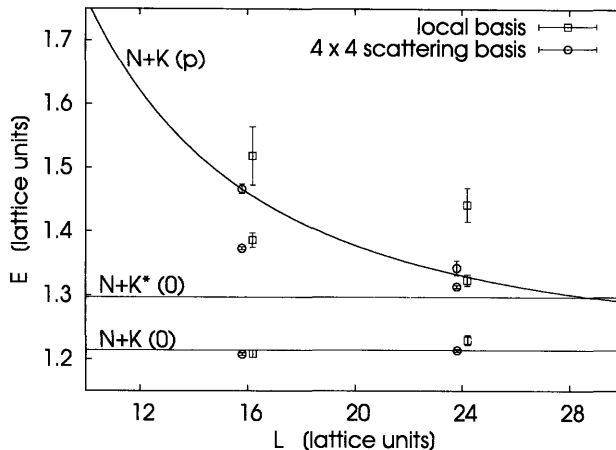
Figure 7-1: Volume dependence of lowest three states for negative parity.

consistent with those of the scattering basis for this state. Since the spectroscopic analysis is based on the variational principle, it is expected that approximation of a delocalized scattering state in a local basis will yield a higher energy than a delocalized basis. Unlike the ground state case, the local basis contains no specific states corresponding to $K^* - N$ scattering states, so the local basis decomposition by itself does not provide a clear signature of the structure of the first excited state. Thus, all the evidence indicates that the observed state is a $K^* - N$ scattering state.

For the second excited state, the scattering basis decomposition indicates that it is a $K - N$ scattering state, since it is dominated by the $K - N$ operator with the smallest non-zero relative momentum. This is confirmed by the energy fits in the scattering basis, which in this case agree with the free scattering states at both volumes. The calculations in the local basis have much larger error bars than the scattering basis, as one expects for a trial function with a small overlap with the eigenstate, and yield energies clearly higher than the scattering basis, as one expects from the variational principle. Hence, all the evidence indicates that the observed state is a $K - N$ scattering state.

Therefore, we have shown that all the states in the energy region we have considered are scattering states and that there are no localized pentaquark states in this region.
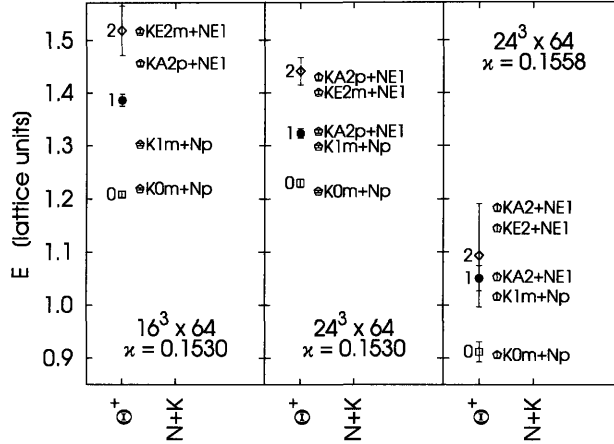
Figure 7-2: Comparison of energies of lowest three states against the relevant hadron states (refer to Tab. 2.5 for non-zero momentum notation).

For the lighter quark mass, we have performed the local basis analysis, but not the scattering basis analysis. The results are shown in Fig. 7-2. The first two columns are a restatement of the heavy quark results, whereas the rightmost column shows the light quark results. For the ground state, we confirm the observation of a $K - N$ scattering state both from the energy fit and operator decomposition. Like in the heavy quark case, decomposition does not provide a clear signature of the state for the first two excited states. The energy fit for the first excited state is consistent with the sum of K^* and N energies, but the second excited state has a big statistical error.

The two major limitations of our calculation were the quenched approximation and heavy quark masses. Although the techniques developed in the work provide a methodology to analyze very light quark masses, the computer resources available at the time did not allow for such a calculation. The problem is two-fold: light quark analyses need higher statistics, while the cost per configuration grows significantly. One also needs a well-defined transfer matrix to perform diagonalization in any basis, and it is problematic for Domain Wall fermions.

Bibliography

[1] D. Diakonov, V. Petrov and M. V. Polyakov, Z. Phys. A **359** (1997) 305 [arXiv:hep-ph/9703373].

[2] S. Eidelman *et al.* [Particle Data Group], Phys. Lett. B **592**, 1 (2004) and 2005 partial update for the 2006 edition available on the PDG WWW pages (URL:hkttp://pdg.lbl.gov).

[3] M. Danilov, arXiv:hep-ex/0509012.

[4] R. A. Schumacher, arXiv:nucl-ex/0512042.

[5] V. D. Burkert, Int. J. Mod. Phys. A **21**, 1764 (2006) [arXiv:hep-ph/0510309].

[6] Invited talk at Elba Workshop on Electron-Nuicleus Scattering IX, Elba, June 2006

[7] T. Nakano, "Recent results of LEPS at SPring-8" Nucl. Phys. A **721**, 112c (2003).

[8] N. Baltzell *et al.*, to be submitted to Phys Rev. Lett.; reported by V. Burkert at the Lepton Photon Conference, Uppsala, Sweden, July, 2005.

[9] S. Stepanyan *et al.* [CLAS Collaboration], "Observation of an exotic S = +1 baryon in exclusive photoproduction from the deuteron," Phys. Rev. Lett. **91**, 252001 (2003) [arXiv:hep-ex/0307018].

[10] T. Nakano *et al.*, Deuterium result from LEPS/SPring-8 (2004) (unpublished).

[11] T. Nakano *et al.*, International Conference on QCD and Hadronic Physics, Beijing, June 2005.

[12] J. Barth *et al.* [SAPHIR Collaboration], "Observation of the positive-strangeness pentaquark Θ^+ in photoproduction with the SAPHIR detector at ELSA," Phys. Lett. B **572**, 127 (2003).

[13] M. Battaglieri *et al.* [CLAS Collaboration], Phys. Rev. Lett. **96**, 042001 (2006) [arXiv:hep-ex/0510061].

[14] V. Kubarovsky *et al.* [CLAS], "Observation of an exotic baryon with S = +1 in photoproduction from the proton," Phys. Rev. Lett. **92**, 032001 (2004) [Erratum-ibid. **92**, 049902 (2004)].

[15] V. V. Barmin *et al.* [DIANA Collaboration], "Observation of a baryon resonance with positive strangeness in K^+ collisions with Xe nuclei," Phys. Atom. Nucl. **66**, 1715 (2003).

[16] K. Abe *et al.* [Belle Collaboration], "Search for the $\Theta(1540)^+$ pentaquark using kaon secondary interactions at Belle," arXiv:hep-ex/0507014.

[17] M. Abdel-Bary *et al.* [COSY-TOF], "Evidence for a narrow resonance at 1530 MeV/c^2 in the $K^0 p$-system of the reaction $pp \rightarrow \Sigma^+ K^0 p$ from the COSY-TOF experiment," Phys. Lett. B **595**, 127 (2004).

[18] A. Airapetian *et al.* [HERMES Collaboration], "Evidence for a narrow $|S| = 1$ baryon state at a mass of 1528-MeV in quasi-real photoproduction," Phys. Lett. B **585**, 213 (2004) [arXiv:hep-ex/0312044].

[19] S. Chekanov *et al.* [ZEUS Collaboration], "Evidence for a narrow baryonic state decaying to $K^0_S p$ and $K^0_S \bar{p}$ in deep inelastic scattering at HERA," Phys. Lett. B **591**, 7 (2004).

[20] K. Gotzen [BaBar Collaboration], "Search for pentaquarks at BABAR," arXiv:hep-ex/0510041.

[21] T. Berger-Hryn'ova [BABAR Collaboration], AIP Conf. Proc. **814**, 320 (2006) [arXiv:hep-ex/0510044].

[22] A. Aleev *et al.* [SVD Collaboration], "Observation of narrow baryon resonance decaying into p K0(S) in p A Phys. Atom. Nucl. **68**, 974 (2005) [Yad. Fiz. **68**, 1012 (2005)] [arXiv:hep-ex/0401024].

[23] A. Aleev *et al.* [SVD Collaboration], "Further study of narrow baryon resonance decaying into K0(S) p in p A arXiv:hep-ex/0509033.

[24] M. I. Adamovich *et al.* [WA89 Collaboration], "Search for the pentaquark candidate $\Theta(1540)^+$ in the hyperon beam experiment WA89," Phys. Rev. C **72**, 055201 (2005); arXiv:hep-ex/0510013.

[25] Y. M. Antipov *et al.* [SPHINX Collaboration], "Search for $\Theta(1540)^+$ in exclusive proton-induced reaction $p + C(N) \to \Theta^+ \overline{K^0} + C(N)$ at the energy of 70 GeV," Eur. Phys. J. A **21**, 455 (2004).

[26] M. J. Longo *et al.* [HyperCP Collaboration], "High statistics search for the $\Theta^+(1.54)$ pentaquark," Phys. Rev. D **70**, 111101 (2004) [arXiv:hep-ex/0410027].

[27] I. Abt *et al.* [HERA-B Collaboration], "Limits for the central production of Θ^+ and Ξ^{--} pentaquarks in 920-GeV pA collisions," Phys. Rev. Lett. **93**, 212003 (2004) [arXiv:hep-ex/0408048].

[28] J. Z. Bai *et al.* [BES Collaboration], "Search for the pentaquark state in $\psi(2S)$ and J/ψ decays to $K_S^0 p K^- \overline{n}$ and $K_S^0 \overline{p} K^+ n$," Phys. Rev. D **70**, 012004 (2004) [arXiv:hep-ex/0402012].

[29] D. O. Litvintsev [CDF Collaboration], "Pentaquark searches at CDF," Nucl. Phys. Proc. Suppl. **142**, 374 (2005) [arXiv:hep-ex/0410024].

[30] S. Schael *et al.* [ALEPH], "Search for pentaquark states in Z decays," Phys. Lett. B **599**, 1 (2004).

[31] R. L. Jaffe and F. Wilczek, Phys. Rev. Lett. **91** (2003) 232003 [arXiv:hep-ph/0307341].

[32] F. Csikor, Z. Fodor, S. D. Katz and T. G. Kovacs, JHEP **0311**, 070 (2003) [arXiv:hep-lat/0309090].

[33] S. Sasaki, Phys. Rev. Lett. **93**, 152001 (2004) [arXiv:hep-lat/0310014].

[34] T. W. Chiu and T. H. Hsieh, arXiv:hep-ph/0403020.

[35] N. Mathur *et al.*, Phys. Rev. D **70**, 074508 (2004) [arXiv:hep-ph/0406196].

[36] N. Ishii, T. Doi, H. Iida, M. Oka, F. Okiharu and H. Suganuma, arXiv:hep-lat/0408030.

[37] C. Alexandrou, G. Koutsou and A. Tsapalis, arXiv:hep-lat/0409065.

[38] T. T. Takahashi, T. Umeda, T. Onogi and T. Kunihiro, arXiv:hep-lat/0410025.

[39] B. G. Lasscock *et al.*, Phys. Rev. D **72**, 014502 (2005) [arXiv:hep-lat/0503008].

[40] F. Csikor, Z. Fodor, S. D. Katz, T. G. Kovacs and B. C. Toth, arXiv:hep-lat/0503012.

[41] C. Alexandrou and A. Tsapalis, arXiv:hep-lat/0503013.

[42] T. T. Takahashi, T. Umeda, T. Onogi and T. Kunihiro, Phys. Rev. D **71**, 114509 (2005) [arXiv:hep-lat/0503019].

[43] K. Holland and K. J. Juge [BGR (Bern-Graz-Regensburg) Collaboration], Phys. Rev. D **73**, 074505 (2006) [arXiv:hep-lat/0504007].

[44] O. Jahn, J. W. Negele and D. Sigaev, PoS **LAT2005**, 069 (2006) [arXiv:hep-lat/0509102].

[45] C. Michael, Nucl. Phys. B **259** (1985) 58.

[46] M. Lüscher and U. Wolff, Nucl. Phys. B **339** (1990) 222.

[47] M. Lüscher, Commun. Math. Phys. **54** (1977) 283.

[48] Y. Liang, K. F. Liu, B. A. Li, S. J. Dong and K. Ishikawa, Phys. Lett. B **307**, 375 (1993) [arXiv:hep-lat/9304011].

[49] D. C. Moore and G. T. Fleming, Phys. Rev. D **73**, 014504 (2006) [arXiv:hep-lat/0507018].

[50] D. C. Moore and G. T. Fleming, Phys. Rev. D **74**, 054504 (2006) [arXiv:hep-lat/0607004].